Entanglement in $2p$ atom pairs in H_2 photodissociation as studied by measuring the angular correlation function of Lyman-α photon pairs on a whole sphere

Yutaro Torizuka,[1] Kouichi Hosaka,[2,1] Philipp Schmidt,[3] Takeshi Odagiri,[4] Arno Ehresmann,[3] Masashi Kitajima,[1] and Noriyuki Kouchi[1,*]

[1]*Department of Chemistry, Tokyo Institute of Technology, Meguro-ku, Tokyo 152-8551, Japan*

[2]*Quantum Materials and Applications Research Center, National Institutes for Quantum Science and Technology (QST), Takasaki, Gunma 370-1292, Japan*

[3]*Institute of Physics and Center for Interdisciplinary Nanostructure Science and Technology (CINSaT), University of Kassel, Heinrich-Plett-Straβe 40, D-34132 Kassel, Germany*

[4]*Department of Materials and Life Sciences, Sophia University, Chiyoda-ku, Tokyo 102-8554, Japan*

(Received 8 November 2024; accepted 23 January 2025; published 21 February 2025)

An angular correlation function (ACF) of a pair of Lyman-α photons produced in photodissociation of H_2 with linearly polarized incident light is measured on a whole sphere at a 33.66-eV photon energy so that we may distinctly substantiate that the $2p$ atom pairs are in the state previously identified by Torizuka *et al.* as the $2p$ atom-pair state [Phys. Rev. A **99**, 063426 (2019)], who measured the ACF only on a circle in the plane perpendicular to the incident light beam. The $2p$ atom-pair state determined with much less uncertainty than before is investigated in terms of whether or not the state is entangled. We discover that the pair of fragment H($2p$) atoms is certainly entangled in terms of the electron-electron entanglement, and obtain the entanglement entropy of the $2p$ atom-pair state. The similar discussion is made in terms of the electronic spatial-spin entanglement too, where the spatial motion and spin motion of electrons are considered nonidentical partial systems at variance with the former electron-electron entanglement. It turns out that the pair of fragment H($2p$) atoms is entangled in terms of the electronic spatial-spin entanglement as well as the electron-electron entanglement.

DOI: 10.1103/PhysRevA.111.023116

I. INTRODUCTION

Entanglement is an intrinsic concept in quantum mechanics [1]. It has been extensively used as a resource for quantum information technology [2], and the investigation on entanglement has expanded into the fields adjacent to quantum information as well [3]. The entanglement will play a significant role in atomic and molecular processes and it is a fascinating subject to investigate those processes in terms of the change of entanglement measures for the composite systems involved. As for dissociation of molecules, Miyagi *et al.* [4] and Jänkälä *et al.* [5] have predicted that entangled pairs of H($2p$) atoms are produced through the breakup of H_2 molecules in the doubly excited $Q_2\,{}^1\Pi_u(1)$ state and have shown that the entanglement may be substantiated with measuring the angular correlation function (ACF) of a pair of Lyman-α photons.

The photodissociation process of H_2 into H($2p$) + H($2p$) was at first investigated with measuring the cross section for emitting a pair of Lyman-α photons against the incident photon energy in the range 30–44 eV [6], and the cross section was measured also for D_2 [7] and HD [8] as well as H_2 in terms of the isotope effect. Recently, the same cross section curve was measured again for H_2 [9], which result is in agreement with the earlier ones. It has been well substantiated from those cross-section curves as well as theoretical investigations, e.g., Ref. [10], that H($2p$) atom pairs are produced and decayed through the following process:

$$\begin{aligned} H_2\left(X\,{}^1\Sigma_g^+\right) + \gamma_{\rm ex} &\rightarrow H_2[Q_2\,{}^1\Pi_u(1)] \text{ in the FC region} \\ &\rightarrow H(2p) + H(2p) \\ &\rightarrow H(1s) + H(1s) + \gamma_{\text{Ly-}\alpha} + \gamma_{\text{Ly-}\alpha}, \end{aligned} \quad (1)$$

where $\gamma_{\rm ex}$ is a linearly polarized incident photon, $\gamma_{\text{Ly-}\alpha}$ a Lyman-α photon, and "FC region" stands for the Franck-Condon region. Typical distance between the two H($2p$) atoms in process (1) reaches 93 μm at a 33.66-eV incident photon energy when they emit the Lyman-α photons [11]. The formation of a pair of H($2p$) atoms is a suitable subject for investigating whether or not the molecular dissociation can produce entangled atom pairs because most of the $2p$ atom pairs originate from the $Q_2\,{}^1\Pi_u(1)$ state in the photoexcitation of H_2 in the range of the incident photon energy 30–44 eV. The potential energy curve and resonance width of the doubly excited $Q_2\,{}^1\Pi_u(1)$ state have been calculated against the internuclear distance in the range below $6a_0$ [12,13]. The theoretical investigations by Miyagi *et al.* [4] and Jänkälä *et al.* [5] are early ones in the next phase of the cross-section measurements mentioned above.

Inspired by Refs. [4,5], Tanabe *et al.* [14,15] and Nakanishi *et al.* [16] measured the ACF of Lyman-α photon pairs at

*Contact author: nkouchi@chem.titech.ac.jp

a 33.66-eV incident photon energy, which gives a maximum cross section for emitting Lyman-α photon pairs [6–9], to find out that the experimental ACFs, contrary to the expectation, are not in agreement with the theoretical ACFs in Refs. [4,5]. Torizuka *et al.* [11] have measured the ACF of Lyman-α photon pairs at a 33.66-eV incident photon energy again, but in a wider angular range at a narrower angular step with smaller distortion than in Refs. [14–16]. From the ACF, Torizuka *et al.* [11] have identified the state of a $2p$ atom pair to be not the $Q_2\,{}^1\Pi_u(1)$ state but the superposition of the $Q_2\,{}^1\Pi_u(1)$ and $Q_2\,{}^3\Sigma_u^+(2)$ state. However, Torizuka *et al.* [11], as well as previous authors [14–16], have measured the ACF only on a circle in the plane perpendicular to the linearly polarized incident light beam, the circle which is termed a dipole circle according to Ref. [5], and there remains a possibility that the experimental ACF does not coincide with the theoretical ACF derived from the $2p$ atom-pair state identified by Torizuka *et al.* [11] out of the dipole circle. The reason for the possibility is as follows. It has been shown based on the analytical expression of the ACF [17] that it is impossible to derive the ACF on a whole sphere from the ACF on the dipole circle. The agreement on the dipole circle does not hence ensure the agreement on other regions. We consequently aim at measuring the ACF of Lyman-α photon pairs on a whole sphere to examine whether the experimental ACF coincides with the theoretical one by Torizuka *et al.* [11] over the whole sphere. The state of $2p$ atom pairs may be determined with much less uncertainty through the ACF of Lyman-α photon pairs on the whole sphere than through the ACF simply measured only on the dipole circle. We also aim at determining whether or not the state of $2p$ atom pairs is entangled along the established criterion mentioned in the Appendix. We try to investigate entanglement of the precursor molecular state of the $2p$ atom pairs too taking advantage of the known electron configuration of the state. It is a fascinating subject to investigate the change of entanglement during dissociation.

Regarding the types of entanglement, we discuss two types: one is the electron-electron entanglement and the other is the electronic spatial-spin entanglement. In the former entanglement, the two electrons in two-electron systems under study are partial systems, which are identical particles, and, in the latter entanglement, the spatial motion and spin motion of those electrons are considered two partial systems, which are not identical "particles."

Recently, Dochain *et al.* [9] measured the relative ACF of Lyman-α photon pairs at three points within the dipole circle with the linearly polarized incident light at a 33.6-eV photon energy and calculated the ACF on a relative scale in the same angular range as in Ref. [11]. Their experimental and theoretical results are not so contradictory with those by Torizuka *et al.* [11] in terms of shape. However, their method for calculating the ACF is in remarkable contrast with the method used by Torizuka *et al.* [11] in terms of how to write the $2p$ atom-pair state and how to calculate the probability density for the simultaneous detection of two photons (Torizuka *et al.* have used the same method as the present one). The comparison with the study by Dochain *et al.* [9] is referred to in Sec. IV.

This paper is organized as follows. Section I is followed by Sec. II, where we describe an overview in Sec. II A, setups in Sec. II B, and the procedure for obtaining the ACF on a whole sphere step by step in detail in Sec. II C. In Sec. III, the experimental ACF on a whole sphere is obtained. The part of discussion is divided into two sections, i.e., Secs. IV and V. In Sec. IV, the state of $2p$ atom pairs is definitely identified, and in Sec. V, the entanglement of the $2p$ atom-pair state is investigated as well as that of the precursor molecular state of the pair. In Sec. VI, we conclude this paper with summarizing what has been achieved. The Appendix is a preparation for Sec. V, in which we review entanglement in two-electron systems.

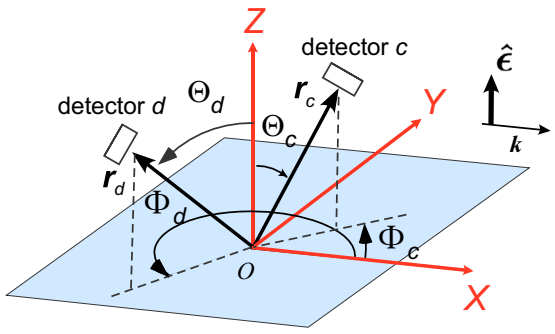

FIG. 1. The space-fixed XYZ frame. $\hat{\boldsymbol{\epsilon}}$: the unit polarization vector of the linearly polarized incident light, $\boldsymbol{k}$: the wave-number vector of the incident light. See Sec. II A for details. Produced with revising Fig. 1(b) in Ref. [17].

II. EXPERIMENTS

A. An overview

The experiments were carried out at the bending beam line BL20A [18] of the Photon Factory, Institute of Materials Structure Science, KEK, as in the early experiments [11,14–16]. The linearly polarized light was used with a 33.66-eV photon energy and 140-meV energy width. The principle for measuring the ACF on a whole sphere is based on the general expression of the ACF, which is a superposition of cosine functions of four angular variables specifying the directions of two detectors and involves five coefficients [17]. In order to obtain the ACF on a whole sphere, we may just measure the ACF in a sufficiently wide range of the angles to determine those coefficients.

We introduce a frame of reference held fixed to the incident light beam, termed the space-fixed frame (see Fig. 1). The origin O of the space-fixed XYZ frame is taken on the incident light beam. The incident light travels down the positive direction of the X axis, and the positive direction of the Z axis points to the direction of the unit polarization vector of the linearly polarized incident light $\hat{\boldsymbol{\epsilon}}$. The Y axis is taken so that the space-fixed XYZ frame is a right-handed system. We arrange two photon detectors with respect to the space-fixed frame, detectors which are labeled c and d. The direction of each detector is specified by the Euler angles $(\Phi_{c/d}, \Theta_{c/d}, \Psi_{c/d} = 0)$ as seen in Fig. 1, provided that each detector is originally on the $+Z$ axis. This definition of the detector angles $(\Theta_{c/d}, \Phi_{c/d})$ is the same as in [4,11,14–17].

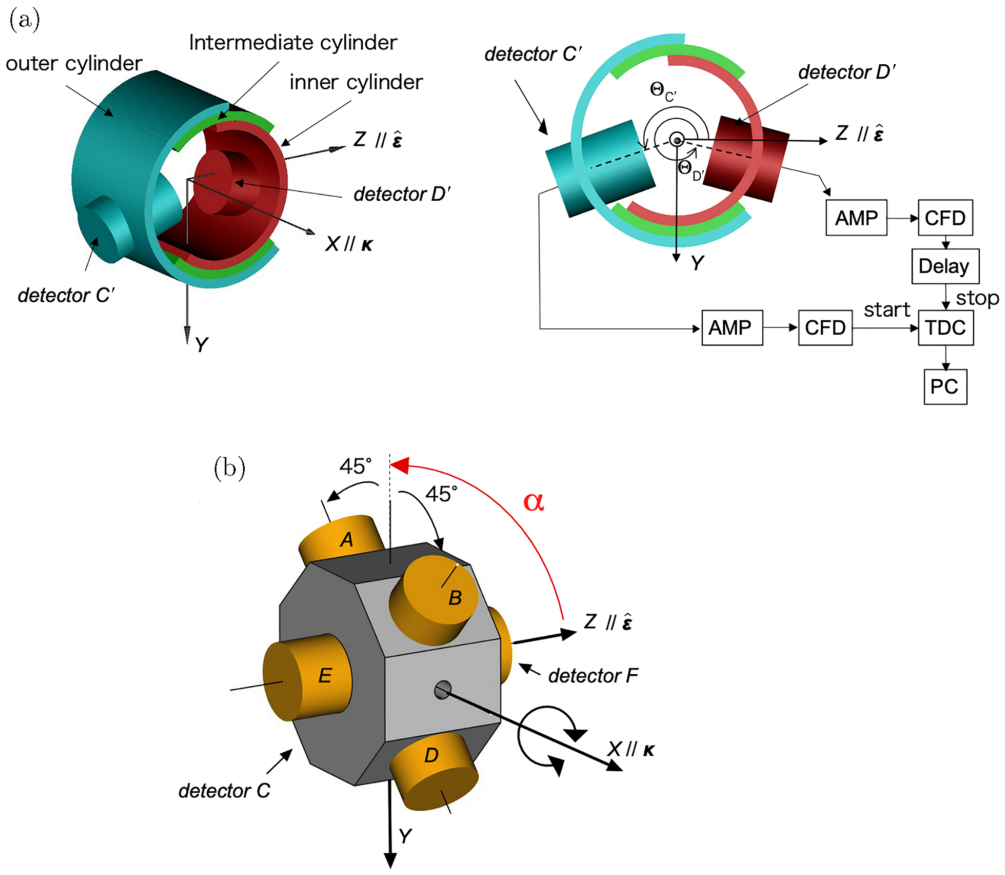

FIG. 2. The detector arrangement in setup 1 (a) and setup 2 (b). (a) The detector arrangement on the gas cell as well as the coincidence system in setup 1. (b) The detector arrangement on the gas cell in setup 2. The same as Fig. 1 about $\hat{\boldsymbol{\epsilon}}$ and $\boldsymbol{k}$. In (b), the detector C, positioned to face in opposite direction to the detector B, is hidden by the gas cell. The positive directions of $\Theta_{C'}$, $\Theta_{D'}$, and α, which are measured from $\hat{\boldsymbol{\epsilon}}$, are shown. AMP: amplifier; CFD: constant-fraction discriminator; TDC: time-to-digital converter; PC: personal computer. (a) Reproduced from Fig. 1 in Ref. [11].

We use the convention that $\Phi_{c/d} = \frac{3}{2}\pi$ if the detector is on the dipole circle.

B. Experimental setups

We obtain the ACF on a whole sphere from the result out of the dipole circle in this experiment and that on the dipole circle in Ref. [11]. Both results were obtained with separate setups. The setup used in the present experiment is referred to as setup 2 while that used by Torizuka *et al.* [11] is referred to as setup 1. Setup 2, as well as setup 1, is described for explaining how to obtain the ACF on a whole sphere, but the description of setup 1 is given where necessary. Setup 1 is equipped with a cylindrical gas cell and setup 2 is equipped with an octagonal prism gas cell, on which cells photon detectors are put. The detector arrangement in setups 1 and 2 is illustrated diagrammatically in Fig. 2. The configuration of the photon detectors in setup 2 is the same as in setup 1, and refer to Ref. [11] for the reason why we have concluded that only Lyman-α photons, with a 121.6-nm wavelength for H atoms, are detected at a 33.66-eV incident photon energy. The solid angles subtended by the detectors in setup 2 are 0.21 sr and those by the detectors in setup 1 are 0.64 sr, where the detectors are seen from the origin of the space-fixed XYZ frame. The flux of incident photons passing through an exit of the gas cell in setups 1 and 2 was recorded with measuring photocurrent of an Au plate, not shown in Fig. 2.

Setup 2 is equipped with six detectors labeled A–F: A–D are put out of the dipole circle while E and F are put on it as seen in Fig. 2(b). The detectors A–F are rotated as a whole over the incident light beam and let the rotation angle be denoted by α, which is measured from the unit polarization vector of the linearly polarized incident light $\hat{\boldsymbol{\epsilon}}$ as shown in Fig. 2(b) with the positive direction of the angle α being shown. The direction of the vector $\hat{\boldsymbol{\epsilon}}$ was experimentally determined with the measurement of the angular distribution of photoelectrons from He such as in setup 1 in the manner described in Ref. [16]. The apparatus for this measurement is not shown in Fig. 2.

Setup 1 is equipped with two detectors, labeled C' and D', and they are put on the dipole circle. At variance with setup 2, the detectors are rotated independently over the incident light beam. In the early study with setup 1, the detector labels c and d referred to the specific detectors in setup 1 [11, 14–16]. However, in this paper, the labels c and d are a type of variables, and the variables c and d refer to any of the specific detectors A–F, C', and D' throughout setups 1 and 2 (in Sec. II A, the detector labels c and d are used in this sense). The transformation from the rotation angle α of the gas cell in

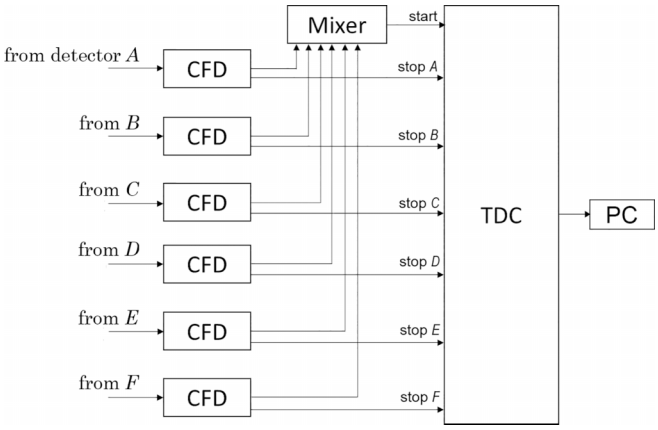

FIG. 3. The block diagram of the system for simultaneously measuring the coincidence time spectra for all the pairs of the detectors in setup 2. The same as Fig. 2 about CFD, TDC, and PC.

setup 2 to (Θ_c, Φ_c) is readily derived for $c = A$–F, where α ranges from -180° to 180°.

In experiments with the static gas target being used, the sample gas pressure in the gas cell should be carefully chosen so that the reactions of $H(n = 2)$ atoms with hydrogen molecules do not affect the ACF. It has been discovered from thoroughly examining the proportionality of the two-photon coincidence count rate to the H_2 gas pressure that the reactions do not play a role in the pressure range lower than ~2 Pa. The experiments with setup 2, as well as setup 1, were carried out at pressures of ~1 Pa within a variation of ±5%.

The arrival time of a Lyman-α photon at each detector in setup 2 is recorded with the system shown in Fig. 3 so that we can build up the coincidence time spectra for all the pairs of detectors simultaneously. The coincidence system in setup 1 is shown in Fig. 2(a). See Fig. 2 in Ref. [11] as for an example of coincidence time spectra. The accidental coincidence counts, as well as the contribution of cascade from $H(n \geqslant 3)$ to $H(2p)$, are subtracted in the manner described in detail in the early paper [16]. The false coincidence counts due to cosmic muons [16] were sufficiently low in comparison with the true coincidence counts so that the false ones were not subtracted, which is the same as in the experiments with setup 1 [11].

C. Procedure to obtain the ACF on a whole sphere

There are 15 pairs of the detectors in setup 2 and we measure 15 ACFs as a function of the angle α (the number of combinations to choose 2 from 6 is 15). We write, for example, (A, B) for the pair of detectors A and B. According to the analytical expression of the ACF [17], those 15 pairs are divided into the following four groups so that all the pairs in each group give the same ACF as a function of α:

(1) $\{(A, B), (C, D), (A, C), (B, D)\}$, referred to as the AB group;

(2) $\{(A, D), (B, C)\}$, referred to as the AD group;

(3) $\{(A, E), (A, F), (B, E), (B, F), (C, E), (C, F), (D, E), (D, F)\}$, referred to as the AE group;

(4) (E, F).

The AB, AD, and AE groups give the ACFs out of the dipole circle, but the EF pair gives the ACF on the dipole circle.

First, we measure the relative ACFs for the AB group, AD group, AE group, and the EF pair as a function of α with setup 2. In addition to those four ACFs, we have in our hands three relative ACFs early measured on the dipole circle as a function of $\Theta_{C'}$ with setup 1 [11]. However, not all of those seven ACFs are put on the same relative scale of the vertical axis. Hence, second, we unify many relative scales of the vertical axis to one relative scale, and eventually obtain the ACF on a whole sphere on the absolute scale in units of sr^{-2}. In Secs. II C 1–II C 3, the procedure is mentioned at each stage.

1. Measuring the ACFs on separate vertical scales

This stage was mentioned in Ref. [11], but in terms of only setup 1. It is thus mentioned here in a general way. We start with the relation between the two-photon coincidence count rate $\dot{N}_{cd}(\Theta_c, \Phi_c, \Theta_d, \Phi_d)$, abbreviated to $\dot{N}_{cd}(\Omega_c, \Omega_d)$, and the angle-differential cross section for emitting a pair of Lyman-α photons, denoted by $d^2\sigma/d\Omega\, d\Omega' = q(\Omega, \Omega')$, because $q(\Omega, \Omega')$ divided by the angle-integrated cross section σ is equal to the ACF:

$$\frac{\dot{N}_{cd}(\Omega_c, \Omega_d)}{P \times i_{\mathrm{Au}}(\Omega_c, \Omega_d)} = C(\Omega_c, \Omega_d)\, G_{cd}(\Omega_c, \Omega_d)\, \eta_c\, \eta_d\, \langle q \rangle(\Omega_c, \Omega_d). \quad (2)$$

The incident photon energy is held fixed at 33.66 eV in the experiments with setups 1 and 2. In the right-hand side of Eq. (2), $\langle q \rangle$ is the angle-differential cross section averaged with the angular resolution, $C(\Omega_c, \Omega_d)$ an instrumental constant, and $\eta_{c(d)}$ a detection efficiency of the photon detector $c(d)$ for a Lyman-α photon. A geometric factor $G_{cd}(\Omega_c, \Omega_d)$ is an integral of (*the detector c solid angle*) × (*the d solid angle*) over the interval of the gas cell on the X axis. The geometric factor $G_{cd}(\Omega_c, \Omega_d)$ and instrumental constant $C(\Omega_c, \Omega_d)$ are independent of (Ω_c, Ω_d) if the detectors c and d are rotated over the incident light beam such as in setups 1 and 2. In the left-hand side of Eq. (2), P is pressure of hydrogen gas in the gas cell and i_{Au} is the photocurrent from the Au plate located below the exit hole of the gas cell, both quantities which are measured in setups 1 and 2. However, it is difficult to measure the four quantities other than $\langle q \rangle(\Omega_c, \Omega_d)$ in the right-hand side. We hence carry out the reference measurement at a fixed arrangement of the detectors so that we can cancel those four quantities taking advantage of the independence of $G_{cd}(\Omega_c, \Omega_d)$ and $C(\Omega_c, \Omega_d)$ of (Ω_c, Ω_d) as seen below:

$$\frac{\dot{N}_{cd}(\Omega_c, \Omega_d)/[P \times i_{\mathrm{Au}}(\Omega_c, \Omega_d)]}{\dot{N}^R_{cd}(\Omega^R_c, \Omega^R_d)/\left[P^R \times i^R_{\mathrm{Au}}(\Omega^R_c, \Omega^R_d)\right]} = \frac{\langle q \rangle(\Omega_c, \Omega_d)}{\langle q \rangle(\Omega^R_c, \Omega^R_d)}, \quad (3)$$

where the quantities with a superscript "R" refer to those in reference measurements. We choose the reference arrangement (Ω^R_c, Ω^R_d) as follows: for the measurement with setup

1 ($c = C'$ and $d = D'$) [11],

$$\left(\Omega^R_{C'}, \Omega^R_{D'}\right) = \left(\Theta^R_{C'} = -\frac{\pi}{2},\ \Phi^R_{C'} = \frac{3}{2}\pi,\ \Theta^R_{D'} = \frac{\pi}{2},\ \Phi^R_{D'} = \frac{3}{2}\pi\right), \tag{4}$$

and for the measurement with setup 2 [$c(d) = A$–F and $c \neq d$],

$$\left(\Omega^R_c, \Omega^R_d\right) = \left(\Theta^R_c(\alpha = 0),\ \Phi^R_c(\alpha = 0),\ \Theta^R_d(\alpha = 0),\ \Phi^R_d(\alpha = 0)\right). \tag{5}$$

In fact, we use

$$\frac{\dot{N}_{cd}(\Omega_c, \Omega_d)/[P \times i_{\mathrm{Au}}(\Omega_c, \Omega_d)]}{\frac{1}{2}\left(\left\{\dot{N}^{R'}_{cd}(\Omega^R_c, \Omega^R_d)/\left[P^{R'} \times i^{R'}_{Au}(\Omega^R_c, \Omega^R_d)\right]\right\} + \left\{\dot{N}^{R''}_{cd}(\Omega^R_c, \Omega^R_d)/\left[P^{R''} \times i^{R''}_{Au}(\Omega^R_c, \Omega^R_d)\right]\right\}\right)} = \frac{\langle q\rangle(\Omega_c, \Omega_d)}{\langle q\rangle(\Omega^R_c, \Omega^R_d)}, \tag{6}$$

instead of Eq. (3): the $\dot{N}_{cd}$ measurement is carried out between the $\dot{N}^{R'}_{cd}$ and $\dot{N}^{R''}_{cd}$ reference measurements.

Let the left-hand side of Eq. (6) as a whole be denoted by $R_{cd}(\Omega_c, \Omega_d; \Omega^R_c, \Omega^R_d)$ so that $R_{cd}(\Omega_c, \Omega_d; \Omega^R_c, \Omega^R_d)$ is an ACF as a function of (Ω_c, Ω_d) on the relative scale with reference to $\langle q\rangle(\Omega^R_c, \Omega^R_d)$ [the reference arrangement (Ω^R_c, Ω^R_d) is held fixed]. We can thereby obtain several ACFs on separate relative scales at separate ranges of detector angles with setups 1 and 2 as follows:

$$R_{C'D'}\left(\Omega_{C'}, \Omega_{D'}; \Omega^R_{C'}, \Omega^R_{D'}\right) \quad \text{vs } (\Theta_{C'}, \Theta_{D'}), \tag{7a}$$

$$R_{cd}\left(\Omega_c(\alpha), \Omega_d(\alpha); \Omega^R_c, \Omega^R_d\right) \quad \text{vs } \alpha \quad \text{for } (c, d) \in AB, AD, \text{ and } AE \text{ groups}, \tag{7b}$$

$$R_{EF}\left(\Omega_E(\alpha), \Omega_F(\alpha); \Omega^R_E, \Omega^R_F\right) \quad \text{vs } \alpha, \tag{7c}$$

where $(\Omega_{C'}, \Omega_{D'})$ in Eq. (7a) stands for $(\Theta_{C'}, \frac{3}{2}\pi, \Theta_{D'}, \frac{3}{2}\pi)$. Equations (7a) and (7c) are the relative ACFs on the dipole circle and Eq. (7b) is the relative ACFs out of the dipole circle.

As seen in Eq. (2), we measure not $q(\Omega_c, \Omega_d)$ but $\langle q\rangle(\Omega_c, \Omega_d)$, which is averaged $q(\Omega_c, \Omega_d)$ with the angular resolution. We have carefully examined the influence of the angular resolution on the angular averaging in setup 2 experiments to discover that the equation $\langle q\rangle(\Omega_c, \Omega_d) = q(\Omega_c, \Omega_d)$ holds to a good approximation for the ACFs shown in this article including those measured with setup 1 but it fails to hold for $\langle q\rangle(\Omega_A, \Omega_C)$ and $\langle q\rangle(\Omega_B, \Omega_D)$, both of which belong to the AB group. The results for the AC pair and BD pair in the AB group are hence excluded from panel (3) in Fig. 4 [panel (3) is for the AB group], but those for the AB pair and CD pair remain there.

2. *Unifying the vertical scales in the ACFs*

In order to match the relative scales in Eqs. (7b) and (7c) to the relative scale in Eq. (7a), we obtain the ratios of reference cross sections $\langle q\rangle(\Omega^R_c, \Omega^R_d)/\langle q\rangle(\Omega^R_{C'}, \Omega^R_{D'})$ for $c(d) = A$–F and $c \neq d$ so that the ratios act as a unification factor as shown below: the ACF,

$$\overbrace{\left(\frac{\langle q\rangle\left(\Omega^R_c, \Omega^R_d\right)}{\langle q\rangle\left(\Omega^R_{C'}, \Omega^R_{D'}\right)}\right)}^{\text{the ratio}} R_{cd}\left(\Omega_c(\alpha), \Omega_d(\alpha); \Omega^R_c, \Omega^R_d\right) = \frac{\langle q\rangle(\Omega_c(\alpha), \Omega_d(\alpha))}{\langle q\rangle\left(\Omega^R_{C'}, \Omega^R_{D'}\right)} \text{ vs } \alpha,$$

in setup 2 [$c(d) = A$–F and $c \neq d$] and the ACF in Eq. (7a) in setup 1 are the ACFs on the unified relative scale of the vertical axis with reference to only $\langle q\rangle(\Omega^R_{C'}, \Omega^R_{D'})$. Our principle for obtaining the unification factor $\langle q\rangle(\Omega^R_c, \Omega^R_d)/\langle q\rangle(\Omega^R_{C'}, \Omega^R_{D'})$ is that we search for a special angular coordinate on the dipole circle $(\tilde{\Theta}^{(c,d)}_{C'}, \frac{3}{2}\pi, \tilde{\Theta}^{(c,d)}_{D'}, \frac{3}{2}\pi)$ that satisfies $q(\Omega^R_c, \Omega^R_d) = q(\tilde{\Theta}^{(c,d)}_{C'}, \frac{3}{2}\pi, \tilde{\Theta}^{(c,d)}_{D'}, \frac{3}{2}\pi)$ for each (c, d) with $c(d) = A$–F and $c \neq d$. Such angular coordinates have been actually discovered and we have obtained the unification factors within the ACF on the dipole circle. The discovery of the special angular coordinates enables us to obtain the unification factors without the procedure of unifying the vertical scales. In searching for such $(\tilde{\Theta}^{(c,d)}_{C'}, \frac{3}{2}\pi, \tilde{\Theta}^{(c,d)}_{D'}, \frac{3}{2}\pi)$, we use an analytical expression of the ACF [17] and the invariance of the ACF under the rotation around the Z axis (see Sec. IV A in Ref. [17]). We can thereby obtain seven ACFs on the unified relative scale as seen in Fig. 4 (at this stage, consider the scale of the vertical axis the unified relative one), the four of ACFs which are measured with setup 2 in this experiment [◯ in panels (3)–(6)] and the remaining three have been measured with setup 1 [△ in panels (1) and (2)] [11]. We arrange the two ACFs for $\Theta_{D'} = -\Theta_{C'}$ and $\Theta_{D'} = -\Theta_{C'} + \pi$ together in panel (2) since it has turned out from the analytical expression of the ACF [17] that those ACFs are the same.

We need the relative values at $\Theta_{C'} = -\frac{3}{4}\pi, -\frac{\pi}{4}, \frac{\pi}{4}, \frac{3}{4}\pi$ in reference to the value at $\Theta_{C'} = -\frac{\pi}{2}$ in panel (2) in Fig. 4 to obtain the unification factors for panels (3) and (5), but those experimental points are missing because setup 1 has the limitation that $|\Theta_{C'} - \Theta_{D'}| \geqslant 120^\circ$ [11]. Those missing values are restored with the linear interpolation near the missing points in panel (2).

3. *The ACF on a whole sphere*

In order to obtain the ACF on the absolute scale in units of sr^{-2} on a whole sphere from the ACFs on the unified relative scale, symbols in Fig. 4, we introduce the analytical expression of the ACF on a relative scale [17]

$$\begin{aligned} f^r(\Theta_c, \Phi_c, \Theta_d, \Phi_d) &= k^r_1 + k^r_2(\cos 2\Theta_c + \cos 2\Theta_d) \\ &\quad + k^r_3[\cos 2(\Theta_c - \Theta_d) + \cos 2(\Theta_c + \Theta_d)] \\ &\quad + 2k^r_4 \cos(\Phi_c - \Phi_d)[\cos 2(\Theta_c - \Theta_d) - \cos 2(\Theta_c + \Theta_d)] \end{aligned}$$

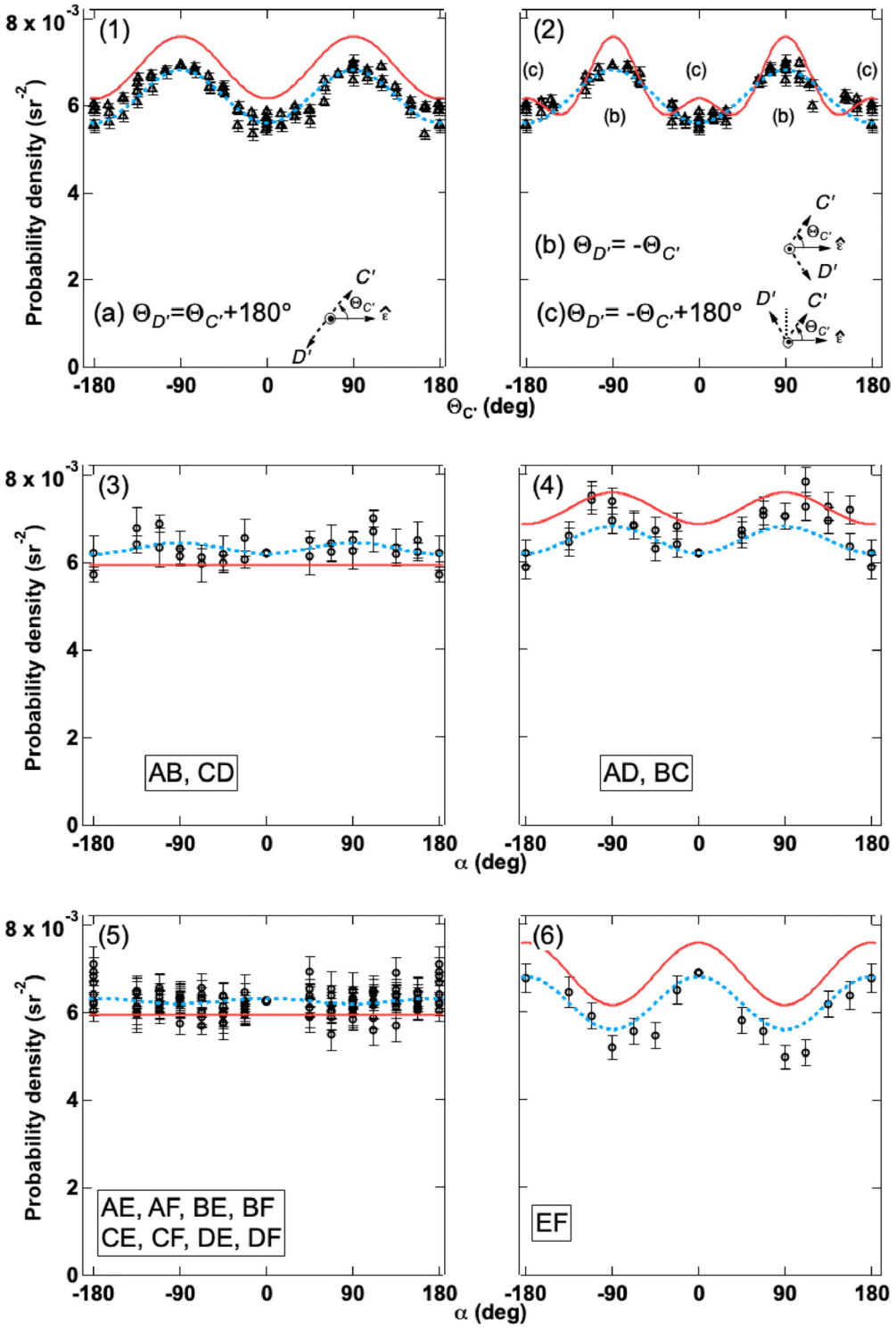

FIG. 4. The experimental ACF [symbols and dashed curve (light blue)] and theoretical ACF (red solid curve) originating from the $|1_u; \eta, R \to \infty\rangle$ state in Eq. (24). The symbols (△) in panels (1) and (2) were measured with setup 1 [11], and the symbols (◯) in panels (3)–(6) have been measured in this experiment. The scale of the vertical axis is not a relative one but absolute one. In panels (3)–(6), for example, the symbol *AB* stands for the pair of detectors *A* and *B*, and the pairs in the same panel give the same ACF as a function of the angle α. Refer to the beginning of Sec. II C for details.

$$+ 2k_5^r \cos 2(\Phi_c - \Phi_d)[2 - 2\cos 2\Theta_c - 2\cos 2\Theta_d + \cos 2(\Theta_c - \Theta_d) + \cos 2(\Theta_c + \Theta_d)], \quad (8)$$

where k_1^r–k_5^r are coefficients independent of (Ω_c, Ω_d). Integrating $f^r(\Theta_c, \Phi_c, \Theta_d, \Phi_d)$ over the whole range of the solid

angles yields

$$\int_{\Theta_c=0}^{\pi}\int_{\Phi_c=0}^{2\pi}\int_{\Theta_d=0}^{\pi}\int_{\Phi_d=0}^{2\pi} f^r(\Theta_c,\Phi_c,\Theta_d,\Phi_d)\,d\Omega_c\,d\Omega_d = \left(k_1^r-\frac{2}{3}k_2^r+\frac{2}{9}k_3^r\right)(4\pi)^2. \tag{9}$$

Hereafter, $\int\ldots d\Omega_c\,d\Omega_d$ means integrating over the whole range of the solid angles.

In order to discuss how to determine five coefficients k_1^r–k_5^r in $f^r(\Omega_c,\Omega_d)$, we write the ACFs in Eqs. (7) based upon $f^r(\Omega_c,\Omega_d)$ in Eq. (8) as follows [the ACFs in Eqs. (7) are on the separate relative scales of the vertical axis, but those below are on the unified relative scale]:

$$f^r\left(\Theta_{C'},\tfrac{3}{2}\pi,\Theta_{C'}+\pi,\tfrac{3}{2}\pi\right) = a_1^r+4a_2^r\cos^2\Theta_{C'}+8a_3^r\cos^4\Theta_{C'}, \tag{10}$$

$$f^r\left(\Theta_{C'},\tfrac{3}{2}\pi,-\Theta_{C'},\tfrac{3}{2}\pi\right) = b_1^r+4b_2^r\cos^2\Theta_{C'}+8b_3^r\cos^4\Theta_{C'}, \tag{11}$$

$$f^r\left(\Theta_{C'},\tfrac{3}{2}\pi,-\Theta_{C'}+\pi,\tfrac{3}{2}\pi\right) = b_1^r+4b_2^r\cos^2\Theta_{C'}+8b_3^r\cos^4\Theta_{C'}, \tag{12}$$

$$f^r(\Theta_A(\alpha),\Phi_A(\alpha),\Theta_B(\alpha),\Phi_B(\alpha)) = c_1^r+2c_2^r\cos^2\alpha+2c_3^r\cos^4\alpha, \tag{13}$$

$$f^r(\Theta_A(\alpha),\Phi_A(\alpha),\Theta_E(\alpha),\Phi_E(\alpha)) = d_1^r+d_2^r\cos^2\alpha+4d_3^r\cos^4\alpha, \tag{14}$$

where Eqs. (10)–(12) correspond to the ACFs on the dipole circle in Eq. (7a), and Eqs. (13) and (14) to the ACFs out of the dipole circle in Eq. (7b). The coefficients a_i^r, b_i^r, c_i^r, and d_i^r $(i=1,2,3)$ are expressed as linear combinations of k_1^r–k_5^r in Eq. (8). The reason why $f^r(\Omega_A(\alpha),\Omega_D(\alpha))$ and $f^r(\Omega_E(\alpha),\Omega_F(\alpha))$ are not considered is that the former ACF turns out to be a part of the ACF in Eq. (10) in the interval $[45^\circ,135^\circ]$ and the latter ACF is equivalent with the ACF in Eq. (10).

The coefficients a_1^r–a_3^r, b_1^r–b_3^r, c_1^r–c_3^r, and d_1^r–d_3^r in Eqs. (10)–(14) are obtained with fitting the ACFs in those equations to the corresponding experimental ACFs on the unified relative scale in Fig. 4 (symbols) obtained in the stage of Sec. II C 2. It has turned out that the coefficients k_1^r–k_5^r in Eq. (8) are expressed as linear combinations of a_1^r–a_3^r, b_1^r–b_3^r, c_1^r–c_3^r, and d_1^r–d_3^r, which fact shows that the present angular range is sufficiently wide to determine the coefficients k_1^r–k_5^r in Eq. (8). We have hence fitted $f^r(\Theta_c,\Phi_c,\Theta_d,\Phi_d)$ in Eq. (8) to all the experimental ACFs on the unified relative scale in Fig. 4 (symbols) after converting those experimental ACFs (symbols) to functions of $(\Theta_c,\Phi_c,\Theta_d,\Phi_d)$, and have obtained the values of k_1^r–k_5^r. On the other hand, it has turned out to be impossible to determine the coefficients k_1^r–k_5^r from only the ACF on the dipole circle. Once the coefficients k_1^r–k_5^r in Eq. (8) are obtained, the ACF on the absolute scale in units of sr^{-2} on a whole sphere, $\frac{dP}{d\Omega_c\,d\Omega_d}(\Omega_c,\Omega_d)$, is given by [see Eq. (9)]

$$\frac{dP}{d\Omega_c\,d\Omega_d}(\Omega_c,\Omega_d) = \frac{1}{\left(k_1^r-\frac{2}{3}k_2^r+\frac{2}{9}k_3^r\right)(4\pi)^2}\times f^r(\Theta_c,\Phi_c,\Theta_d,\Phi_d). \tag{15}$$

Note that $f^r(\Omega_c,\Omega_d)$ includes the coefficients k_1^r–k_5^r. In deriving Eq. (15), we use the normalization relation that integrating an ACF over the whole sphere yields unity. The symbols on the unified relative scale in Fig. 4 have been ultimately put on the absolute scale in units of sr^{-2} with multiplying the relative values of symbols by the factor $\frac{1}{[k_1^r-(2/3)k_2^r+(2/9)k_3^r](4\pi)^2}$ in Eq. (15).

III. RESULTS

In order to show the experimental ACF on a whole sphere on the absolute scale, we introduce an analytical expression of the ACF in units of sr^{-2} in explicit form [17]

$$\begin{aligned}\frac{dP}{d\Omega_c\,d\Omega_d}(\Omega_c,\Omega_d) = \frac{1}{(4\pi)^2}\{&a_1+a_2(\cos2\Theta_c+\cos2\Theta_d)+a_3[\cos2(\Theta_c-\Theta_d)+\cos2(\Theta_c+\Theta_d)]\\&+2a_4\cos(\Phi_c-\Phi_d)[\cos2(\Theta_c-\Theta_d)-\cos2(\Theta_c+\Theta_d)]\\&+2a_5\cos2(\Phi_c-\Phi_d)[2-2\cos2\Theta_c-2\cos2\Theta_d+\cos2(\Theta_c-\Theta_d)+\cos2(\Theta_c+\Theta_d)]\},\\ &a_1-\frac{2}{3}a_2+\frac{2}{9}a_3=1.\end{aligned} \tag{16}$$

Here, the combination of both equations is equivalent to Eq. (15). The ACF in Eq. (16) is simply specified by a 1×5 matrix

$$(a_1,a_2,a_3,2a_4,2a_5). \tag{17}$$

We use this matrix to express the ACF as a function of the four angular variables.

In Fig. 4, shown is the graph of the experimental ACF on a whole sphere in units of sr^{-2} (dashed line), i.e., the graph of $dP/d\Omega_c d\Omega_d$ in Eq. (15) with the values of k_1^r–k_5^r determined through the fit of Eq. (8) to the experimental data (symbols) on the unified relative scale as mentioned in Sec. II C 3. The explicit expression of the dashed line in the form of Eq. (17) is

$$\begin{aligned}&(a_1,a_2,a_3,2a_4,2a_5)_{\mathrm{Expt}}\\&=(0.974\pm0.002,\ -(3.9\pm0.2)\times10^{-2},\\&\quad(2\pm1)\times10^{-3},\ (3.2\pm1.7)\times10^{-3},\\&\quad(4.7\pm0.5)\times10^{-3})_{\mathrm{Expt}}.\end{aligned} \tag{18}$$

Also shown in Fig. 4 (symbols) is another experimental ACF in units of sr^{-2}, the ACF which is obtained with the manner mentioned at the last part of Sec. II C 3.

The uncertainty in the ACF is in the order of $10^{-3}/(4\pi)^2$ sr^{-2} as seen in Eq. (18), and is much smaller than the constant and dominant component due to a_1. The anisotropy of the ACF is not so strong as seen in Eq. (18): a_1 is much larger than the absolute values of others. Recently, three experimental points were reported on a relative scale at $\Theta_{C'} = -180°$, $-135°$, and $-90°$ for the $\Theta_{D'} = \Theta_{C'} + \pi$ arrangement on the dipole circle [9], points which are consistent with the present results in panel (1) in Fig. 4 in terms of shape (see Fig. 13 in Ref. [9]).

IV. IDENTIFYING THE $2p$ ATOM-PAIR STATE: REVISITED

The $2p$ atom-pair state identified by Torizuka *et al.* through the ACF measured on the dipole circle [11] is examined through the present ACF measured on the whole sphere. As mentioned in Ref. [11], our principle is the following:

(i) We prepare a "trial" state of $2p$ atom pairs that is reasonably accessed from the precursor $Q_2\,{}^1\Pi_u(1)$ state in process (1).

(ii) We calculate the theoretical ACF for the trial $2p$ atom-pair state.

(iii) We examine whether or not the theoretical ACF is in agreement with the experimental ACF.

(iv) If the agreement is obtained, we identify that trial state of $2p$ atom pairs as the real $2p$ atom-pair state (the end of task), else we go back to step (i) and keep going until reaching the end of the task.

In this principle, it is essential that trial states of $2p$ atom pairs are physically reasonable and the method of calculating ACFs is appropriate. The experimental ACF with which the theoretical ACF is compared was the one measured only on the dipole circle in the previous study [11] while it is the one measured on the whole sphere in this study. As mentioned above, we start with a pure ensemble. If it does not work, we consider a mixed ensemble. In Sec. IV A, we review the identification by Torizuka *et al.* [11] to find out several issues in step (i) above, issues which we resolve in Sec. IV B.

We write electronic states of H_2 molecules relying on the Born-Oppenheimer approximation. For this purpose, we introduce one more frame of reference held fixed to the protons in the molecule, termed the molecular frame, as shown in Fig. 5 besides the space-fixed XYZ frame in Fig. 1. We label the two electrons 1 and 2 and the two protons a and b. The z axis in the molecular xyz frame points from proton a to b as shown in Fig. 5 with those protons at rest with respect to the space-fixed frame. The origin of the molecular frame is taken at the midpoint between protons a and b, and is taken to coincide with the origin of the space-fixed XYZ frame. The molecular xyz frame is specified with respect to the space-fixed XYZ frame with the Euler angles $(\phi, \theta, 0)$ as seen in Fig. 5 ($0 \leqslant \phi \leqslant 2\pi$ and $0 \leqslant \theta \leqslant \pi$). Electronic states of H_2 molecules are written with reference to the molecular frame, and hence parametrically involve the relative position vector of the two protons $\boldsymbol{R}$ [$\boldsymbol{R} = (R, \theta, \phi)$ and R denotes internuclear distance]. The orbital angular momentum of electrons is denoted by $\hat{\boldsymbol{L}}$, the spin angular momentum of electrons by $\hat{\boldsymbol{S}}$, and the sum of them by $\hat{\boldsymbol{J}}$, where the atomic unit is used. As will be seen in due course, electronic states of H_2 as $\hat{J}_z$ eigenstates are considered at $R \to \infty$ while those as simultaneous eigenstates of $\hat{L}_z$ and $\hat{S}_z$ are considered in the Franck-Condon region. The nuclear motion is not taken into account.

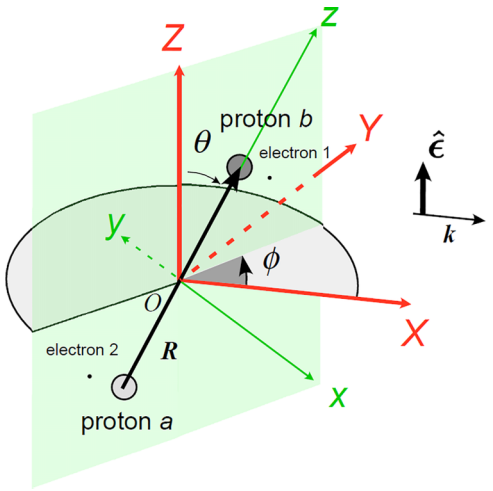

FIG. 5. The molecular xyz frame as well as the space-fixed XYZ frame. The same as Fig. 1 about $\hat{\boldsymbol{\epsilon}}$ and $\boldsymbol{k}$. See Sec. IV for details. Produced with revising Fig. 1(a) in Ref. [17].

In the calculation of the ACF by our group [4,11,17], we assume that the molecular xyz frame of an H_2 molecule not having absorbed an incident photon is randomly oriented with respect to the space-fixed XYZ frame and the molecular frame of an H_2 molecule having absorbed an incident photon does not rotate against the space-fixed frame during the dissociation into $\mathrm{H}(2p) + \mathrm{H}(2p)$, which assumptions fit with the present experiment as well as the early ones [11,14–16].

A. Review of the identification in Ref. [11]

Staring from the ACF measured only on the dipole circle, and after testing several trial states, Torizuka *et al.* [11] have identified the $2p$ atom-pair state as an 1_u state at infinite internuclear distance. The 1_u state at $R \to \infty$, denoted by $|1_u; \eta, \eta_{\mathrm{SO}}, R \to \infty\rangle$, is given as [11]

$$|1_u; \eta, \eta_{\mathrm{SO}}, R \to \infty\rangle = \frac{1}{\sqrt{2}}\left\{ \left|{}^3\Sigma_u^+; R \to \infty\right\rangle \left[\frac{1}{\sqrt{2}}\left(\left|\chi^e_{11}\right\rangle - e^{i\eta}\left|\chi^e_{1-1}\right\rangle\right)\right] \right.$$
$$\left. - e^{-i\eta_{\mathrm{SO}}}\left[\frac{1}{\sqrt{2}}\left(\left|{}^1\Pi_u^{L_z=+1}; R \to \infty\right\rangle + e^{i\eta}\left|{}^1\Pi_u^{L_z=-1}; R \to \infty\right\rangle\right)\right]\left|\chi^e_{00}\right\rangle \right\}, \tag{19}$$

TABLE I. The entanglement entropies of the $2p$ atom-pair state ($R \to \infty$) and precursor molecular state ($R = R_e$) in the H_2 photodissociation as well as the united-atom He state ($R = 0$).

Internuclear distance	$R = 0$	$R = R_e$	$R \to \infty$	min	max[a]
			A. Electron-electron entanglement		
Offset entanglement entropy[b]	1.1[c]	1	1.718[d]	0	3[e]
Slater rank		2	6	1	8
			B. Spatial-spin entanglement		
Entanglement entropy	0	0	1	0	2[f]
Schmidt rank	1	1	2	1	4

[a] The maxima refer to only $R = R_e$ and $R \to \infty$.
[b] A measure for two-electron systems (see Appendix, Sec. 2).
[c] From Ref. [22].
[d] $(17/6) + \log_2 3 + (1/\sqrt{6})\log_2(49 - 20\sqrt{6}) = 1.718$.
[e] $\log_2(d/2)$, where $d = 16$. See Appendix, Sec. 2.
[f] $\log_2 d$, where $d = 4$. See Appendix, Sec. 1.

where $0 \leqslant \eta \leqslant 2\pi$ (it is a last trial state and has eventually been identified as the real $2p$ atom-pair state). Here, the $|^3\Sigma_u^+; R \to \infty\rangle$ state is given by Eq. (29) in Ref. [11], the $|^1\Pi_u^{L_z=\pm1}; R \to \infty\rangle$ states by Eq. (7) in Ref. [11], and the spin eigenstates for the two-electron system, $|\chi^e_{S=0,S_z=0}\rangle$ and $|\chi^e_{1\pm1}\rangle$, by Eqs. (6), (30), and (31) in Ref. [11] (the $|\chi^e_{00}\rangle$ state is the singlet state and the $|\chi^e_{1\pm1}\rangle$ states are two states of the three triplet states in total). The $|\chi^e_{10}\rangle$ state, another triplet state, does not occur because the $|^3\Sigma_u^+; R \to \infty\rangle|\chi^e_{10}\rangle$ state is a 0_u state. The $|^3\Sigma_u^+; R \to \infty\rangle$ and $|^1\Pi_u^{L_z=\pm1}; R \to \infty\rangle$ states have been antisymmetrized and symmetrized, respectively, with respect to the permutation operator of electrons 1 and 2 so that the $|1_u; \eta, \eta_{\rm SO}, R \to \infty\rangle$ state is antisymmetric. The symbol $\eta_{\rm SO}$ denotes the phase angle of the matrix element,

$$\left\langle {}^3\Sigma_u^+; R \to \infty \middle| \langle \chi^e_{11} | \hat{H}^{\rm SO}(R \to \infty) \middle| {}^1\Pi_u^{L_z=+1}; R \to \infty \right\rangle | \chi^e_{00} \rangle, \tag{20}$$

where $\hat{H}^{\rm SO}(R)$ expresses the spin-orbit coupling in a hydrogen molecule at internuclear distance R [11], and $\eta_{\rm SO}$ turns out to be zero in this study as mentioned later while it was unknown in Ref. [11]. The 1_u state is a superposition of the $Q_2\,{}^1\Pi_u(1)$ and $Q_2\,{}^3\Sigma_u^+(2)$ states. The reason why such a superposition occurs has been mentioned in Ref. [11], but will be investigated again in an exact way when solving the two-state problem between those two states later. Note that Torizuka *et al.* [11], as well as we, have not intended to write entangled $2p$ atom-pair states, but have just written the states so that they possess the characteristics that they should possess.

The $|1_u; \eta, \eta_{\rm SO}, R \to \infty\rangle$ state is, in fact, dependent on (θ, ϕ), which specifies the molecular xyz frame with respect to the space-fixed XYZ frame, but the (θ, ϕ) dependence is restricted to the ket vectors and the coefficients in the superposition are not dependent on (θ, ϕ) in the right-hand side of Eq. (19). The reason why the coefficients are not dependent on (θ, ϕ) is that in process (1) the processes proceed in the same manner irrespective of (θ, ϕ) after the photoexcitation [17]. Because of such a fact about the (θ, ϕ) dependence as well as simplicity, the (θ, ϕ) dependence is not shown explicitly in Eq. (19). In what follows, we omit the (θ, ϕ) dependence in state vectors as long as no confusion occurs.

Torizuka *et al.* [11] have used two approximations to get to the 1_u state in Eq. (19). One is solving the two-state problem between the $Q_2\,{}^1\Pi_u(1)$ state and $Q_2\,{}^3\Sigma_u^+(2)$ state as J_z eigenstates instead of solving the nine-state problem among the nine 1_u states shown in Table I in Ref. [11], where the doubly excited Q_2 states correlating with the $n = 2 + n = 2$ dissociation limit are listed, and the other is using the strong-coupling approximation in solving the two-state problem, the approximation that the magnitude of the difference of the diagonal matrix elements in the 2×2 Hamiltonian matrix of the two-state problem is neglected against the magnitudes of the off-diagonal matrix elements. The reason why such an approximation has been adopted is that the eigenstates are readily obtained without complicated calculations even though those eigenstates are approximate. The validity of the latter approximation has not been substantiated while the former approximation has been sufficiently justified [11], and let us rigorously solve the two-state problems between the $|^3\Sigma_u^+; R \to \infty\rangle|\chi^e_{1\pm1}\rangle$ state and $|^1\Pi_u^{L_z=\pm1}; R \to \infty\rangle|\chi^e_{00}\rangle$ state without resorting to the strong-coupling approximation (double sign corresponds). Depending on the results, the coefficients in the superposition in Eq. (19) may change: in Eq. (19) the two states are superposed with the equal weight. The value of $\eta_{\rm SO}$ is obtained in the course of solving the problems.

B. Trial $2p$ atom-pair state obtained with exactly solving the two-state problems

The electronic Hamiltonian $\hat{H}^{\rm ele}(R)$ of a hydrogen molecule is written at internuclear distance R as

$$\hat{H}^{\rm ele}(R) = \hat{H}_0^{\rm ele}(R) + \hat{H}^{\rm SO}(R), \tag{21}$$

where $\hat{H}_0^{\rm ele}(R)$ is the electronic Hamiltonian with only the Coulomb interaction being considered. The 2×2 representation matrices of $\hat{H}^{\rm ele}(R\to\infty)$ in terms of the bases $\{|^3\Sigma_u^+;R\to\infty\rangle|\chi^e_{1\pm1}\rangle, |^1\Pi_u^{L_z=\pm1};R\to\infty\rangle|\chi^e_{00}\rangle\}$ are calculated as

$$\begin{pmatrix} \langle^3\Sigma_u^+|\langle\chi^e_{1\pm1}|\hat{H}^{\rm SO}|^3\Sigma_u^+\rangle|\chi^e_{1\pm1}\rangle = 0 & \langle^3\Sigma_u^+|\langle\chi^e_{1\pm1}|\hat{H}^{\rm SO}|^1\Pi_u^{L_z=\pm1}\rangle|\chi^e_{00}\rangle = \pm[\alpha^2/(24\sqrt{6})] \\ \langle^1\Pi_u^{L_z=\pm1}|\langle\chi^e_{00}|\hat{H}^{\rm SO}|^3\Sigma_u^+\rangle|\chi^e_{1\pm1}\rangle = \pm[\alpha^2/(24\sqrt{6})] & \langle^1\Pi_u^{L_z=\pm1}|\langle\chi^e_{00}|\hat{H}^{\rm SO}|^1\Pi_u^{L_z=\pm1}\rangle|\chi^e_{00}\rangle = 0 \end{pmatrix}, \tag{22}$$

in atomic unit of energy (double sign corresponds), where "$R\to\infty$" is omitted in the spatial ket and bra vectors and $\hat{H}^{\rm SO}(R\to\infty)$ for simplicity, and α is the fine structure constant. In Eq. (22), the origin of energy is taken at the dissociation limit of $\mathrm{H}(n=2)+\mathrm{H}(n=2)$ with the spin-orbit coupling not being considered, with the dissociation limit which both the $Q_2\,{}^1\Pi_u(1)$ and $Q_2\,{}^3\Sigma_u^+(2)$ states correlate [19]. We refer to the explicit expression of $\hat{H}^{\rm SO}(R)$ in Eq. (3.4.2) on p. 181 in Ref. [20]. We separately solve the two two-state problems for the matrices in Eq. (22) (one is the $J_z=1$ problem and the other is $J_z=-1$ problem). Remarkably, we see from Eq. (22) that the strong-coupling approximation which Torizuka *et al.* [11] have used is strictly valid for both of the $J_z=\pm1$ problems because the magnitude of the difference of the diagonal matrix elements is exactly zero. In other words, the strong-coupling "limit" applies. In addition, we learn from the (1,2) element in the matrix in Eq. (22) for $J_z=1$ that $\eta_{\rm SO}=0$. We remark that there occur the singlet-triplet superpositions between the $J_z=\pm1$ components of the $Q_2\,{}^1\Pi_u(1)$ state and $J_z=\pm1$ components of the $Q_2\,{}^3\Sigma_u^+(2)$ state with the strong-coupling limit at $R\to\infty$ even for H_2 (double sign corresponds). Considering the energy origin in Eq. (22), we find out that the major reason why the spin-orbit coupling is so effective that the singlet-triplet superpositions occur at $R\to\infty$ lies in the degeneracy of the $Q_2\,{}^1\Pi_u(1)$ and $Q_2\,{}^3\Sigma_u^+(2)$ states at $R\to\infty$ without considering the spin-orbit coupling. On the other hand, as well known, such a superposition hardly occurs in the Franck-Condon region for H_2. That is because the potential energy curves of the $Q_2\,{}^1\Pi_u(1)$ and $Q_2\,{}^3\Sigma_u^+(2)$ states without considering the spin-orbit coupling are apart from each other by $\sim$1 eV in the Franck-Condon region [12] and the magnitude of the difference of the diagonal matrix elements dominates the magnitudes of the off-diagonal matrix elements in the 2×2 representation matrix of $\hat{H}^{\rm ele}(R)$ with R being in the Franck-Condon region. Summarizing, the spin-orbit coupling has to be taken into account even in H_2 in the case that the potential energies of the states involved, but without considering the spin-orbit coupling, are equal. This case refers to the present $R\to\infty$ region, and we hence use $\hat{J}_z$ eigenstates there. However, the extremely opposite case refers to the Franck-Condon region, and we do not need to take the spin-orbit coupling into account. We hence use $\hat{L}_z$ and $\hat{S}_z$ eigenstates there.

We then derive the exact and physically meaningful eigenstates in the two-state problems in Eq. (22). There exist a high-energy state and a low-energy one for each of the $J_z=1$ and -1 problems, and we take the one that approaches the $Q_2\,{}^1\Pi_u(1)$ state as the spin-orbit coupling becomes negligible because the precursor doubly excited state of the $2p$ atom pairs is the $Q_2\,{}^1\Pi_u(1)$ state in the Franck-Condon region as shown in process (1). It is the low-energy state that satisfies such a requirement. The low-energy states are shown below for the $J_z=\pm1$ problems,

$$\begin{aligned}|1_u^{J_z=\pm1};R\to\infty\rangle = (1/\sqrt{2})\Big(&|^3\Sigma_u^+;R\to\infty\rangle|\chi^e_{1\pm1}\rangle \\ \mp&|^1\Pi_u^{L_z=\pm1};R\to\infty\rangle|\chi^e_{00}\rangle\Big) \\ &\text{(double sign corresponds).}\end{aligned} \tag{23}$$

We then take the superposition of the $|1_u^{J_z=\pm1};R\to\infty\rangle$ states above as follows ($0\leqslant\eta\leqslant2\pi$):

$$\begin{aligned}|1_u;\eta,R\to\infty\rangle = (1/\sqrt{2})\big(&|1_u^{J_z=1};R\to\infty\rangle \\ -e^{i\eta}&|1_u^{J_z=-1};R\to\infty\rangle\big),\end{aligned} \tag{24}$$

so that the $|1_u;\eta,R\to\infty\rangle$ and $|1_u;\eta+\pi,R\to\infty\rangle$ states compose the set of eigenstates for the permutation operator of protons a and b. The $|1_u;\eta,R\to\infty\rangle$ state hence expresses all the low-energy 1_u states that satisfy the indistinguishability of protons as η ranges from 0 to 2π. In addition, the $|1_u;\eta,R\to\infty\rangle$ state is antisymmetric with respect to the permutation operator of electrons 1 and 2 since, as mentioned below Eq. (19), the $|^3\Sigma_u^+;R\to\infty\rangle$ and $|^1\Pi_u^{L_z=\pm1};R\to\infty\rangle$ states in Eq. (23) are antisymmetric and symmetric, respectively. The $|1_u;\eta,R\to\infty\rangle$ state consequently follows the indistinguishability of identical particles. Summarizing, it is the $|1_u;\eta,R\to\infty\rangle$ state in Eq. (24) that is the exact and physically meaningful eigenstate in the present two-state problems, and we use the state as a trial state of $2p$ atom pairs. This state is the same as the state in Eq. (19) ($\eta_{\rm SO}=0$) based on the strong-coupling approximation since the approximation has ultimately turned out to be strictly valid as mentioned before.

C. Calculation of ACF, comparison with experiment, and state identification

We have then calculated the ACF originating from the $|1_u;\eta,R\to\infty\rangle$ state in Eq. (24) [= the $|1_u;\eta,\eta_{\rm SO}=0,R\to\infty\rangle$ state in Eq. (19)] in the manner mentioned in Ref. [11]. The outline of the manner is described in brief [4,11,17]:

(1) The light field is expressed in the form of photon number states, and the single-photon state for the Lyman-α fluorescence is written using the Weisskopf-Wigner theory.

(2) Each hydrogen atom built on proton a or b emits a Lyman-α photon independently and separately. Refer to the time evolution in each hydrogen atom in Eqs. (8)–(13) in

Ref. [11]. The two-photon two-electron state $|\Phi;\eta\rangle$ in the final stage in process (1) is obtained through the time evolution of the nonphoton two-electron state $|1_u;\eta, R\to\infty\rangle|\text{vac}\rangle$ in the second stage, where the ket-vector $|\text{vac}\rangle$ denotes the vacuum state of light. The $|\Phi;\eta\rangle$ state is explicitly expressed in Eq. (33) in Ref. [11]. The characteristic of the no-photon two-electron state $|1_u;\eta, R\to\infty\rangle|\text{vac}\rangle$ is carried over to the two-photon two-electron state $|\Phi;\eta\rangle$, and the inherited characteristic emerges in the ACF.

(3) The probability density for detecting photon pairs is calculated as a function of detector positions and detection times by means of quantum optics, i.e., the expected value of the operator $\hat{\boldsymbol{E}}_c^{(-)}\hat{\boldsymbol{E}}_d^{(-)}\hat{\boldsymbol{E}}_d^{(+)}\hat{\boldsymbol{E}}_c^{(+)}$, which is an operator with four electric fields aligned in the normal order, is calculated for the two-photon two-electron state $|\Phi;\eta\rangle$, where (θ,ϕ) specifying the internuclear axis is held fixed in the state $|\Phi;\eta\rangle$. The calculated probability density is then averaged with the (θ,ϕ,η)-distribution, and the detector position part of the averaged one yields the ACF of Lyman-α photon pairs originating from the $|1_u;\eta, R\to\infty\rangle$ state. Note that the probability density for detecting photon pairs cannot always be written as a product of the probability densities for detecting each photon [4].

The calculated ACF originating from the $|1_u;\eta, R\to\infty\rangle$ state in Eq. (24) is given in the form of Eq. (17) by

$$\begin{aligned}&(a_1, a_2, a_3, 2a_4, 2a_5)_{\text{Theo}}\\&\quad= (627/640,\ -(3/128),\ 27/1280,\ 3/80,\ 21/1280)_{\text{Theo}}\\&\quad= (0.980,\ -2.34\times10^{-2},\ 2.11\times10^{-2},\ 3.75\times10^{-2},\\&\qquad\times 1.64\times10^{-2})_{\text{Theo}},\end{aligned}\tag{25}$$

and is shown with the solid line (red) in Fig. 4 to compare the solid line with the experimental ACF on a whole sphere [dashed line (light blue)]. The absolute values, not the relative values, of the experimental ACF enable us to compare the calculated and experimental ACFs quantitatively. Equation (25) is equivalent to Eq. (37) in Ref. [11]. Note that the calculated ACF is independent of the value of η_{SO}, which fact is the reason why Torizuka *et al.* [11] were able to calculate the ACF although they did not calculate the value of η_{SO}.

At first glance at Fig. 4, it may appear that, in some places, there are discrepancies slightly larger than experimental errors between the experiment (symbols) and theory (solid line). The error bars in Fig. 4 were evaluated from the statistical uncertainty of each two-photon coincidence count rate in the left-hand side of Eq. (6) using the law of the propagation of errors. There are, in fact, errors due to other sources as well. One of them is the error caused by restoring the missing data that are needed to obtain the unification factors for panels (3) and (5) in Fig. 4 as mentioned in the last paragraph in Sec. II C 2. This error appears to considerably contribute to the discrepancies mentioned above, which observation will now be substantiated. Simply speaking, if data (symbols) in some panel decrease, those in other panels increase because of the normalization relation of the ACF. In this regard, we should note that the experimental data (symbols) are slightly and systematically higher than the theory (solid line) in panels (3) and (5) in Fig. 4 but, conversely, the former are lower than the latter in other panels with almost the same extent as the extent of being high in panels (3) and (5). This fact strongly indicates that our observation is valid, and we conclude that the discrepancies beyond the error bars are attributed to the error caused by restoring the missing data. The experimental ACF (symbols) and theoretical ACF (solid line) are indeed in agreement within the error bars in Fig. 4. Note that such agreement is obtained although the theory involves no adjusting parameters that may change the shape and magnitude of the ACF. The small oscillation in the theoretical ACF around $\Theta_{C'}=0^\circ$ and $\pm180^\circ$ in panel (2) in Fig. 4 is made smeared out in the experimental ACF by the error bars and scattering of data points, scattering which is due to the instability in the position of the incident light beam and is not involved in the error bars.

We then examine the similarity between the experimental ACF (dashed line in Fig. 4), $dP^{\text{Expt}}/d\Omega_c\,d\Omega_d$, given by Eq. (18) and theoretical ACF (solid line in Fig. 4), $dP^{\text{Theo}}/d\Omega_c\,d\Omega_d$, given by Eq. (25) not only in the angular range in Fig. 4 but also over the whole sphere. Comparing $(a_1, a_2, a_3, 2a_4, 2a_5)_{\text{Expt}}$ in Eq. (18) and $(a_1, a_2, a_3, 2a_4, 2a_5)_{\text{Theo}}$ in Eq. (25), we find discrepancies beyond the uncertainties in Eq. (18). As mentioned in the previous paragraph, those discrepancies are attributed to the error caused by restoring the missing data, the error which is not involved in the uncertainties in Eq. (18). We examine the similarity with a different way as well, i.e., we calculate the root mean square of the deviation between the experiment and theory defined as

$$\sigma_{\text{rms}} = \sqrt{\frac{\int[(dP^{\text{Theo}}/d\Omega_c\,d\Omega_d)-(dP^{\text{Expt}}/d\Omega_c\,d\Omega_d)]^2 d\Omega_c\,d\Omega_d}{\int\ d\Omega_c\,d\Omega_d}}.\tag{26}$$

The value of σ_{rms} is to be compared with the dominant contribution $a_1/(4\pi)^2$ sr^{-2}, i.e., $1/(4\pi)^2$ sr^{-2}. The value of σ_{rms} is calculated to be $0.046/(4\pi)^2$ sr^{-2}, which is much smaller than $1/(4\pi)^2$ sr^{-2}. The deviation σ_{rms} is mostly due to the error caused by restoring the missing data mentioned in the previous paragraph. It follows from the above that the similarity between the four-variable function $dP^{\text{Expt}}/d\Omega_c\,d\Omega_d$ and $dP^{\text{Theo}}/d\Omega_c\,d\Omega_d$ is satisfactory. Besides, we examine the similarity between $dP^{\text{Ext}}/d\Omega_c\,d\Omega_d$ and $dP^{\text{Theo}}/d\Omega_c\,d\Omega_d$ in terms of how they depend on angular variables. It has been found from Eqs. (18) and (25) that $dP^{\text{Expt}}/d\Omega_c\,d\Omega_d$ and $dP^{\text{Theo}}/d\Omega_c\,d\Omega_d$ have common characteristics as follows:

(a) $a_1 \gg |a_2|, |a_3|, |2a_4|, |2a_5|$ and $a_1\simeq 1$.

(b) The sign of each element in $(a_2, a_3, 2a_4, 2a_5)$, which determines the oscillation around $a_1/(4\pi)^2$ sr^{-2}, is (negative, positive, positive, positive).

It hence turns out that the function $dP^{\text{Expt}}/d\Omega_c\,d\Omega_d$ and $dP^{\text{Theo}}/d\Omega_c\,d\Omega_d$ slightly and synchronously oscillate around $1/(4\pi)^2$ sr^{-2} against the angular variables over the whole sphere [when one increases (decreases), the other also increases (decreases)]. Note that the small oscillation of $dP^{\text{Expt}}/d\Omega_c\,d\Omega_d$ seen in panels (3) and (5) in Fig. 4 appears not to be significant since the amplitude is negligible against the error bars and the oscillation appears to be attributed to the scattering of data points. The function $dP^{\text{Expt}}/d\Omega_c\,d\Omega_d$

will indeed be independent of α in panels (3) and (5) in Fig. 4 such as $dP^{\rm Theo}/d\Omega_c\, d\Omega_d$. We conclude from all the discussions about $(a_1, a_2, a_3, 2a_4, 2a_5)$, $\sigma_{\rm rms}$, and the variable dependence that the four-variable function $dP^{\rm Theo}/d\Omega_c\, d\Omega_d$ and $dP^{\rm Expt}/d\Omega_c\, d\Omega_d$ are sufficiently similar to argue that the former reproduces the latter.

Dochain *et al.* [9] recently calculated the ACF based on the identification of the $2p$ atom-pair state by Torizuka *et al.* [11]. It is the relative ACF calculated in the angular range in panels (1) and (2) in Fig. 4. As mentioned in Secs. I and II C 3, it is impossible to obtain the coefficients a_1–a_5 in Eq. (16) from the ACF on the dipole circle. No large difference is seen between their curve and the present theoretical ACF in terms of shape (see Fig. 13 in Ref. [9]), although minor discrepancies in shape are seen in places in the angular range in panel (2) in Fig. 4. However, we should point out that their calculation method is at very much variance with ours in several respects as mentioned below.

Dochain *et al.* [9] considered the mixed ensemble of 16 1_u states. They showed the list of the eigenvalues of $\hat{L}_z$ and $\hat{S}_z$ for each electron with respect to each 1_u state in their Table I, but showed no explicit expressions of those 1_u states. According to their Table I, the indistinguishability of electrons is likely not to be considered in any 1_u state because the eigenvalues of $\hat{L}_z$ and $\hat{S}_z$ are definite for each electron with respect to each 1_u state as mentioned just above. The indistinguishability of protons is also likely not to be considered in any 1_u state because the superpositions of the $J_z(\tilde{\Omega}$ in their Table I) $= \pm 1$ states are not taken at variance with Eq. (24). On the other hand, we have considered the indistinguishability of electrons and that of protons in writing the $2p$ atom-pair state in Eq. (24), as already mentioned in Secs. IV A and IV B.

Aside from the above, there is a large difference between the method of Dochain *et al.* [9] and ours in calculating the probability density for detecting photon pairs. Dochain *et al.* [9] expressed the probability density for detecting photon pairs as a product of the probability densities for detecting each photon, and calculated the latter probability density for detecting a single photon in the method where fluorescence is considered the electromagnetic wave emitted by an electric dipole. In contrast with Dochain *et al.* [9], we calculate the probability density for detecting photon pairs by means of the two-photon correlation function in quantum optics [see points (1)–(3) mentioned at the beginning of this subsection]. Our method has shown that the probability density for detecting photon pairs cannot always be expressed as a product of the probability densities for detecting each photon [4].

As discussed above, there exist fundamental differences between our method for calculating ACF and that of Dochain *et al.* [9]. Which one to adopt is a difficult question to answer and remains a matter of controversy. In state identification, the validity of theories in use has to be questioned just as much as the agreement or disagreement between experimental results and theoretical predictions. In this paper, as mentioned so far, we have taken the standpoint that the indistinguishability of identical particles should be satisfied at $R \to \infty$. The reason is that both H($2p$) atoms have originated from the same H_2 molecule through its dissociation and it is formal and physically meaningless to label the electrons 1 and 2 and protons a and b, regardless of internuclear distance. In this respect, we note that the experimental ACF in Fig. 4 is free of H_2 gas pressure as mentioned in the second paragraph from the end of Sec. II B. Since we have taken such a standpoint, two-photon two-electron states of the present electronic-photonic system are not always product states of a photonic state and an electronic state, and two-photon states are not always product states of two one-photon states. In such cases, using our method is "safer" than using the method of Dochain *et al.* [9] because according to our method the probability density for detecting photon pairs cannot always be expressed as a product of the probability densities for detecting each photon [4] as above mentioned but Dochain *et al.* [9] write the former probability density as a product of the latter probability densities.

Summarizing, we argue from the sufficient similarity over the whole sphere between $dP^{\rm Expt}/d\Omega_c\, d\Omega_d$ and $dP^{\rm Theo}/d\Omega_c\, d\Omega_d$ calculated in our method that the $2p$ atom pairs in the H_2 photodissociation are in the 1_u state in Eq. (24) [= Eq. (19) with $\eta_{\rm SO} = 0$]. This is the identification of the $2p$ atom-pair state within the framework of our method. However, it is worthwhile to investigate the entanglement of the $2p$ atom-pair state in Eq. (24) based on the physical picture that the dissociating molecule is a molecule.

V. ENTANGLEMENT OF THE 2*p* ATOM-PAIR STATE AND PRECURSOR MOLECULAR STATE

We investigate whether or not the $2p$ atom-pair state in Eq. (24) is entangled, and then derive entanglement measure of the state. We also try to investigate the entanglement of the precursor molecular state of the $2p$ atom pairs as well. The precursor molecular state is the $Q_2\,{}^1\Pi_u(1)$ state at R_e as seen in process (1), where R_e is the equilibrium internuclear distance in the ground electronic state of H_2. In Sec. V A, we argue the electron-electron entanglement with electrons 1 and 2 being considered partial systems. In Sec. V B, we argue the spatial-spin entanglement with the spatial motion and spin motion of electrons being considered two partial systems, which are not identical "particles" in contrast with the electron-electron entanglement in Sec. V A.

In the Appendix, we review what are needed to discuss entanglement. They are the Schmidt decomposition, Schmidt rank, Schmidt coefficient, and entanglement entropy, which refer to two-particle systems whether the particles are identical or not (see the Appendix, Sec. 1). Others are the Slater decomposition, Slater rank, and offset entanglement entropy, which refer to two-electron systems with the indistinguishability of electrons having to be taken into account (see the Appendix, Sec. 2).

A. Electron-electron entanglement

1. The 2p atom-pair state

We investigate the electron-electron entanglement of the $2p$ atom-pair state, the $|1_u; \eta, R \to \infty\rangle$ state in Eq. (24). To

this end, we introduce the linear space for the two-electron system $\bar{\mathcal{H}}(1,2;R\to\infty)$, spanned by a basis $\bar{E}_1\times\bar{E}_2$, where $\bar{E}_i$ (the electron label $i=1,2$) is the orthonormal basis defined as

$$\bar{E}_i=\big\{\big|2p^a_{-1}(i)\big\rangle,\big|2p^a_0(i)\big\rangle,\big|2p^a_{+1}(i)\big\rangle,\big|2p^b_{-1}(i)\big\rangle,\big|2p^b_0(i)\big\rangle,\\ \big|2p^b_{+1}(i)\big\rangle,\big|2s^a(i)\big\rangle,\big|2s^b(i)\big\rangle\big\}\times\big\{\big|\alpha(i)\big\rangle,\big|\beta(i)\big\rangle\big\}\ (i=1,2). \tag{27}$$

Here, for example, the ket vector $|2p^a_{-1}(i)\rangle$ reads that electron i is in the one-electron state $|2p^a_{-1}\rangle$, which is the $2p$ state with $L_z=-1$ built on proton a. The notation |state label (particle label)⟩ keeps being used in this sense from now on. The ket vectors $|\alpha\rangle$ and $|\beta\rangle$ are the spin eigenstates for an electron as usual. The bases $\bar{E}_1\times\bar{E}_2$, $\bar{E}_1$, and $\bar{E}_2$ have been used in Ref. [11], and are referred to as the atomic bases in this paper. The linear space for electron i, $\bar{\mathcal{H}}(i;R\to\infty)$, is spanned by $\bar{E}_i$ $(i=1,2)$ and $\bar{\mathcal{H}}(1,2;R\to\infty)=\bar{\mathcal{H}}(1;R\to\infty)\otimes\bar{\mathcal{H}}(2;R\to\infty)$. We introduce one more basis of $\bar{\mathcal{H}}(1,2;R\to\infty)$, i.e., $\bar{E}'_1(R\to\infty)\times\bar{E}'_2(R\to\infty)$. Here, $\bar{E}'_i(R)$ (the electron label $i=1,2$) is the orthonormal basis defined as

$$\bar{E}'_i(R)=\big\{\big|\pi_u^{-1}\,2p(i);R\big\rangle,\big|\pi_g^{-1}\,2p(i);R\big\rangle,|\sigma_u\,2p(i);R\rangle,|\sigma_g\,2p(i);R\rangle,\big|\pi_u^{+1}\,2p(i);R\big\rangle,\big|\pi_g^{+1}\,2p(i);R\big\rangle,\\ |\sigma_u\,2s(i);R\rangle,|\sigma_g\,2s(i);R\rangle\big\}\times\big\{|\alpha(i)\rangle,|\beta(i)\rangle\big\}(i=1,2). \tag{28}$$

See the correlation diagram between united atom and separated atom states for homonuclear diatomic molecules, e.g., Fig. 10.14 on p. 505 in Ref. [21]. The superscripts ±1 in the π states express the values of L_z. The bases $\bar{E}'_1(R)\times\bar{E}'_2(R)$, $\bar{E}'_1(R)$, and $\bar{E}'_2(R)$ are referred to as the molecular bases. The atomic basis $\bar{E}_i$ and molecular basis $\bar{E}'_i(R\to\infty)$ are related with each other through a unitary matrix. For further description, we introduce the one-electron linear space $\bar{\mathcal{H}}(R)$ and one-electron basis $\bar{E}'(R)$, which are obtained with omitting the electron label i in $\bar{\mathcal{H}}(i;R)$ and $\bar{E}'_i(R)$, respectively. Here, $\bar{\mathcal{H}}(i;R)$ is the linear space for electron i. Summarizing, the dimension d for the space of electron i, $\bar{\mathcal{H}}(i;R)$, is 16 for the electron label $i=1,2$ and $\bar{\mathcal{H}}(1,2;R)=\bar{\mathcal{H}}(1;R)\otimes\bar{\mathcal{H}}(2;R)$ for any R. We discuss the entanglement of the $2p$ atom-pair state and precursor molecular state of $2p$ atom pairs in a unified way with the molecular basis $\bar{E}'_i(R)$ (the electron label $i=1,2$).

We have decomposed the $|1_u;\eta,R\to\infty\rangle$ state in Eq. (24) by means of the Slater decomposition ("$R\to\infty$" is omitted in each one-electron state for simplicity):

$$\begin{aligned}|1_u;\eta,R\to\infty\rangle=&\sqrt{2}\sqrt{p_1^\infty}\left(\frac{1}{\sqrt{2}}\begin{vmatrix}|g2;\eta(1)\rangle & |u2;\eta(1)\rangle\\ |g2;\eta(2)\rangle & |u2;\eta(2)\rangle\end{vmatrix}\right)-\sqrt{2}\sqrt{p_1^\infty}e^{i\eta}\left(\frac{1}{\sqrt{2}}\begin{vmatrix}|g1;\eta(1)\rangle & |u1;\eta(1)\rangle\\ |g1;\eta(2)\rangle & |u1;\eta(2)\rangle\end{vmatrix}\right)\\ &+\sqrt{2}\sqrt{p_2^\infty}\left(\frac{1}{\sqrt{2}}\begin{vmatrix}|u4;\eta(1)\rangle & |g4;\eta(1)\rangle\\ |u4;\eta(2)\rangle & |g4;\eta(2)\rangle\end{vmatrix}\right)-\sqrt{2}\sqrt{p_2^\infty}e^{i\eta}\left(\frac{1}{\sqrt{2}}\begin{vmatrix}|u3;\eta(1)\rangle & |g3;\eta(1)\rangle\\ |u3;\eta(2)\rangle & |g3;\eta(2)\rangle\end{vmatrix}\right)\\ &+\sqrt{2}\sqrt{p_3^\infty}\left(\frac{1}{\sqrt{2}}\begin{vmatrix}|u6;\eta(1)\rangle & |g6;\eta(1)\rangle\\ |u6;\eta(2)\rangle & |g6;\eta(2)\rangle\end{vmatrix}\right)-\sqrt{2}\sqrt{p_3^\infty}e^{i\eta}\left(\frac{1}{\sqrt{2}}\begin{vmatrix}|u5;\eta(1)\rangle & |g5;\eta(1)\rangle\\ |u5;\eta(2)\rangle & |g5;\eta(2)\rangle\end{vmatrix}\right),\end{aligned} \tag{29}$$

where p_1^∞, p_2^∞, and p_3^∞ are the Schmidt coefficients, and specifically

$$p_1^\infty=\left(\frac{3+\sqrt{6}}{12}\right)^2,\quad p_2^\infty=\left(\frac{1}{2\sqrt{6}}\right)^2,\quad p_3^\infty=\left(\frac{3-\sqrt{6}}{12}\right)^2. \tag{30}$$

Here, the one-electron state $|u1;\eta\rangle$, for example, is expressed with a superposition of the elements of $\bar{E}'(R\to\infty)$ as follows:

$$|u1;\eta\rangle=-\tfrac{1}{2}\big|\pi_u^{-1}2p\big\rangle|\alpha\rangle-\tfrac{1}{2}e^{-i\eta}\big|\pi_u^{+1}2p\big\rangle|\alpha\rangle+\tfrac{1}{\sqrt{2}}|\sigma_u2p\rangle|\beta\rangle, \tag{31}$$

where "$R\to\infty$" is omitted in the spatial ket vectors in the right-hand side and "$u1$" reads as the first ungerade state. Equation (29) holds for any η $(0\leqslant\eta\leqslant2\pi)$, i.e., the Schmidt coefficients are independent of η. The one-electron states in Eq. (29), $|u\,j;\eta\rangle$ and $|g\,j;\eta\rangle$ $(j=1-8)$, are normalized and orthogonal to each other.

We immediately find from Eq. (29) that the Slater rank of the $|1_u;\eta,R\to\infty\rangle$ state is 6, and hence conclude that the $|1_u;\eta,R\to\infty\rangle$ state is certainly entangled in terms of the electron-electron entanglement (if "the state's Slater rank" >1, the state is entangled, as seen in the Appendix, Sec. 2). We then obtain the offset entanglement entropy for the $|1_u;\eta,R\to\infty\rangle$ state from Eq. (29) according to the method described in the Appendix, Sec. 2. The offset entanglement entropy is a measure of entanglement of states in two-electron systems (see the Appendix, Sec. 2). The offset entanglement entropy and Slater rank for the $|1_u;\eta,R\to\infty\rangle$ state in terms of the electron-electron entanglement are shown in Table I (the $R\to\infty$ column). It has been substantiated from the Slater rank and offset entanglement entropy that the $2p$ atom-pair state, the $|1_u;\eta,R\to\infty\rangle$ state in Eq. (24), is entangled and the measure of entanglement is considerably large: the offset entanglement entropy amounts up to 57% of the maximum.

The offset entanglement entropy of the $2p$ atom-pair state is influenced by the avoided crossings seen in the potential energy curve of the $Q_2\,{}^1\Pi_u(1)$ state [12], which is the precursor molecular state of the $2p$ atom pairs as seen in process (1), because the $2p$ atom-pair state is the end point of the cumulative histories in the dissociation from the precursor molecular state in the Franck-Condon region up to the $2p$ atom-pair state. In this regard, it is significant to obtain the offset entanglement entropy of the precursor molecular state, which attempt is carried out in the next subsection.

2. The precursor molecular state of the 2p atom pairs

The precursor molecular state is the $Q_2\,{}^1\Pi_u(1)$ state at $R = R_e$ as seen in process (1). The main electron configuration of the $Q_2\,{}^1\Pi_u(1)$ state is known to be $(2p\,\pi_u)(2s\,\sigma_g) = (\pi_u\,2p)(\sigma_g\,2s)$ at R_e [12,23] (the authors of those papers showed only the main configuration). Starting with the main configuration, we write the $Q_2\,{}^1\Pi_u(1)$ state at $R = R_e$ in terms of the molecular basis in Eq. (28) so that the state follows the indistinguishability of electrons and that of protons, which procedure is the same as in deriving the $2p$ atom-pair state in Eq. (24):

$$\left|{}^1\Pi_u;\eta,R_e\right\rangle\left|\chi^e_{00}\right\rangle = \frac{1}{\sqrt{2}}\left(\left|{}^1\Pi_u^{L_z=1};R_e\right\rangle + e^{i\eta}\left|{}^1\Pi_u^{L_z=-1};R_e\right\rangle\right)\left|\chi^e_{00}\right\rangle\ (0\leqslant\eta\leqslant 2\pi), \tag{32}$$

where the $|{}^1\Pi_u^{L_z=\pm1};R_e\rangle$ components of the $Q_2\,{}^1\Pi_u(1)$ state are written as

$$\left|{}^1\Pi_u^{L_z=\pm1};R_e\right\rangle = \tfrac{1}{\sqrt{2}}\left(\left|\pi_u^{\pm1}\,2p(1);R_e\right\rangle|\sigma_g\,2s(2);R_e\rangle + \left|\pi_u^{\pm1}\,2p(2);R_e\right\rangle|\sigma_g\,2s(1);R_e\rangle\right)$$
(double sign corresponds). (33)

The contribution of electronic continua is not taken into account, like the line in calculating entanglement measures for doubly excited states of He atoms [22]. Since the spin-orbit coupling is negligible in comparison with the Coulomb interaction in the Franck-Condon region, the following equation holds:

$$|1_u;\eta,R_e\rangle = \left|{}^1\Pi_u;\eta,R_e\right\rangle\left|\chi^e_{00}\right\rangle. \tag{34}$$

We have decomposed the $|1_u;\eta,R_e\rangle$ state in Eq. (34) by means of the Slater decomposition to obtain the Slater rank and offset entanglement entropy of the state. Those results are shown in Table I (the $R = R_e$ column). The precursor molecular state of the $2p$ atom pairs is entangled in terms of the electron-electron entanglement, but is not as entangled as the $2p$ atom-pair state.

The $Q_2\,{}^1\Pi_u(1)$ state correlates with the doubly excited ${}^1P^o(2s)(2p)$ state of He atoms as $R \to 0$ (the united atom limit) [12]. Cuartas and Sanz-Vicario [22] calculated entanglement measures of doubly excited states of He atoms and found that only the $(2s)(2p)$ configuration was involved in the $|_2(0,1)^+_2,{}^1P^o\rangle$ state, which is the lowest member of the ${}^1P^o$ series converging to the $He^+(n=2)$ ionization threshold. The $Q_2\,{}^1\Pi_u(1)$ state hence turns out to correlate with the $|_2(0,1)^+_2,{}^1P^o\rangle$ state in He atoms as $R \to 0$. The entanglement entropy of this state in He atoms was calculated, but it is the contribution from the spatial part alone [22]. The offset entanglement entropy originating from the spatial and spin parts is shown in Table I (the $R = 0$ column). The $|1_u;\eta,R\to 0\rangle$ state, the $|_2(0,1)^+_2,{}^1P^o\rangle$ state in He atoms, is as entangled as the precursor molecular state of the $2p$ atom pairs in terms of the electron-electron entanglement.

As seen in Table I, the offset entanglement entropy and Slater rank for the $|1_u;\eta,R\rangle$ state increase as internuclear distance R increases from R_e to infinity in terms of the electron-electron entanglement, but it is unknown how they change as a function of R between R_e and infinity. This increase is attributed to the fact that many electron configurations are involved at $R \to \infty$ while the main configuration dominates other ones at R_e. A more detailed discussion on the reason for such increase will be made in a forthcoming article. As a general tendency, we may argue that the larger the multiplicity, the larger the measure of entanglement.

B. Spatial-spin entanglement

1. The 2p atom-pair state

We rewrite the $2p$ atom-pair state in Eq. (19) ($\eta_{\rm SO} = 0$) as

$$|1_u;\eta,\eta_{\rm SO}=0,R\to\infty\rangle = \frac{1}{\sqrt{2}}\left|{}^3\Sigma_u^+;R\to\infty\right\rangle\left[\frac{1}{\sqrt{2}}\left(\left|\chi^e_{11}\right\rangle - e^{i\eta}\left|\chi^e_{1-1}\right\rangle\right)\right] + \frac{1}{\sqrt{2}}\left(-\left|{}^1\Pi_u;\eta,R\to\infty\right\rangle\right)\left|\chi^e_{00}\right\rangle, \tag{35}$$

where the ket vector $|{}^1\Pi_u;\eta,R\to\infty\rangle$ in the right-hand side is defined as $|{}^1\Pi_u;\eta,R\to\infty\rangle = (1/\sqrt{2})(|{}^1\Pi_u^{L_z=1};R\to\infty\rangle + e^{i\eta}|{}^1\Pi_u^{L_z=-1};R\to\infty\rangle)$. We immediately find the $|1_u;\eta,\eta_{\rm SO}=0,R\to\infty\rangle$ state to be expressed in the form of the Schmidt decomposition as it stands because each of the spatial ket vectors occurs only once and they are orthogonal to each other, and the same is seen in the spin ket vectors, which are $[1/\sqrt{2}\,(\dots)]$ and $|\chi^e_{00}\rangle$.

It turns out from Eq. (35) that the Schmidt rank of the $|1_u;\eta,\eta_{\rm SO}=0,R\to\infty\rangle$ state is two and the state is hence entangled in terms of the spatial-spin entanglement (if "the state's Schmidt rank" >1, the state is entangled, as seen in the Appendix, Sec. 1), and the spin-orbit coupling brings about the spatial-spin entanglement. We then obtain the entanglement entropy of the $|1_u;\eta,\eta_{\rm SO}=0,R\to\infty\rangle$ state in Eq. (35) according to the method described in the Appendix, Sec. 1. The entanglement entropy and Schmidt rank of the $|1_u;\eta,\eta_{\rm SO}=0,R\to\infty\rangle$ state in terms of the spatial-spin entanglement are shown in Table I (the $R\to\infty$ column). The $2p$ atom-pair state is entangled too in terms of the spatial-spin entanglement besides the electron-electron entanglement discussed in Sec. V A 1. The entanglement entropy in terms of the spatial-spin entanglement reaches up to 50% of the maximum.

2. The precursor molecular state of the 2p atom pairs

It is obvious that the precursor molecular state, the $|1_u;\eta,R_e\rangle$ state in Eq. (34), is a product state and hence a nonentangled state in terms of the spatial-spin entanglement (see the Appendix, Sec. 1), while it is an entangled state in terms of the electron-electron entanglement as discussed in Sec. V A 2. The entanglement entropy of the $|1_u;\eta,R_e\rangle$ state is hence zero in terms of the spatial-spin entanglement, which result is also shown in Table I as well as the Schmidt rank of the state (the $R = R_e$ column). A product state is possible in the problem of the spatial-spin entanglement at variance with the problem of the electron-electron entanglement since in the former the two motions are not identical "particles" but in the latter electrons are identical.

As mentioned in the second paragraph from the end of Sec. V A 2, the $|1_u;\eta,R\to 0\rangle$ state is the $|_2(0,1)^+_2,{}^1P^o\rangle$ state

in He atoms. The $|1_u;\eta, R\to 0\rangle$ state is hence written as $|\text{spatial}\rangle|\chi^e_{00}\rangle$. The entanglement entropy of the $|1_u;\eta, R\to 0\rangle$ state is consequently zero in terms of the spatial-spin entanglement because of the same reasoning in the $|1_u;\eta, R_e\rangle$ state, which result is shown in Table I as well as the Schmidt rank (the $R=0$ column). The $|1_u;\eta, R\to 0\rangle$ state is a nonentangled state in terms of the spatial-spin entanglement while it is an entangled state in terms of the electron-electron entanglement.

The entanglement entropy and Schmidt rank for the $|1_u;\eta, R\rangle$ state increase as internuclear distance R increases from R_e to infinity in terms of the spatial-spin entanglement as seen in Table I, which increase is attributed to the fact that the $Q_2\,{}^1\Pi_u(1)$ state comes to be superposed with the $Q_2\,{}^3\Sigma^+_u(2)$ state as $R\to\infty$ while they are not superposed around $R=R_e$ as mentioned below Eq. (22). The increasing role of the spin-orbit coupling brings about the increase of the measure of the spatial-spin entanglement for the $|1_u;\eta, R\rangle$ state as the dissociation goes on. Such an increase in the measure of entanglement is another manifestation of the general tendency referred to at the end of Sec. V A 2, i.e., the larger the multiplicity, the larger the measure of entanglement.

VI. CONCLUSION

We have measured the ACF of a Lyman-α photon pair on a whole sphere in the photodissociation of H_2 with linearly polarized light at a 33.66-eV incident photon energy in order to investigate entanglement in the two-electron system and have had significant results as follows.

(a) Considering the atom pair a diatomic molecule with infinite internuclear distance as mentioned in Sec. IV C, we have concluded that the $2p$ atom pairs produced in the photodissociation are in the $|1_u;\eta, R\to\infty\rangle$ state in Eq. (24) $[=|1_u;\eta, \eta_{\rm SO}=0, R\to\infty\rangle$ in Eq. (19)].

(b) We have found out by means of the Slater decomposition that the $2p$ atom-pair state is certainly entangled in terms of the electron-electron entanglement. The offset entanglement entropy of the $2p$ atom-pair state has been obtained and has turned out to reach up to 57% of the maximum. The same discussion has been tried for the precursor molecular state of the $2p$ atom pairs with only the main electron configuration being considered. It has turned out that the precursor molecular state is also entangled in terms of the electron-electron entanglement but is not as entangled as the $2p$ atom-pair state.

(c) We have found out that the $2p$ atom-pair state is entangled also in terms of the electronic spatial-spin entanglement and the entanglement entropy of the state reaches up to 50% of the maximum while the precursor molecular state of the $2p$ atom pairs is not entangled in terms of the spatial-spin entanglement. This large difference between $R\to\infty$ and $R=R_e$ is brought about by the difference in the influence of the spin-orbit coupling on electronic states.

ACKNOWLEDGMENTS

The present experiment was carried out under the approval of the PF IMSS KEK Program Advisory Committee for Proposals No. 2014G108, No. 2016G001, and No. 2018G061. The present investigation has been supported by JSPS KAKENHI Grants No. JP15K05381 and No. JP17K05744. K.H. wishes to thank the financial support from the Yamada Science Foundation and Matsuo Foundation.

APPENDIX: A PREPARATION FOR DISCUSSING ENTANGLEMENT IN TWO-ELECTRON SYSTEMS

In this Appendix, we review entanglement for states of two-electron systems with the indistinguishability of electrons being taken into account (see Secs. 2.6.1 and 3.3 in Ref. [3]), an Appendix which is a preparation for Sec. V. First, the general discussion is briefly made on entanglement in two-particle systems, and then we move on to the discussion on entanglement in two-electron systems.

1. Entanglement in two-particle systems

We consider states of a two-particle system composed of particles 1 and 2. Those particles may or may not be identical. We prepare two d-dimensional linear spaces of one-particle states involved for the particles 1 and 2, spaces which are denoted by $\mathcal{H}(1)$ and $\mathcal{H}(2)$, respectively. For a given state of the two-particle system $|\Psi\rangle\in\mathcal{H}(1)\otimes\mathcal{H}(2)$, it is trivial that the state $|\Psi\rangle$ is expanded through *any* orthonormal bases for $\mathcal{H}(1)$ and $\mathcal{H}(2)$, bases which are $\{|\psi'_i(1)\rangle|i=1,2,\ldots,d\}$ and $\{|\phi'_j(2)\rangle|j=1,2,\ldots,d\}$, respectively: $|\Psi\rangle=\sum_{i,j=1}^d c_{ij}|\psi'_i(1)\rangle|\phi'_j(2)\rangle$, where c_{ij} is a complex number. The number of nonvanishing terms is at most d^2. On the other hand, choosing the *adequate* orthonormal bases of $\mathcal{H}(1)$ and $\mathcal{H}(2)$, i.e., $\{|\psi_i(1)\rangle|i=1,2,\ldots,d\}$ and $\{|\phi_j(2)\rangle|j=1,2,\ldots,d\}$, respectively, it is known that the state $|\Psi\rangle$ may always be decomposed as [3]

$$|\Psi\rangle=\sum_{i=1}^{s}\sqrt{p_i^\Psi}\;|\psi_i(1)\rangle\,|\phi_i(2)\rangle, \tag{A1}$$

where $p_1^\Psi\geqslant p_2^\Psi\geqslant\cdots\geqslant p_s^\Psi>0$. Note the remarkable feature in Eq. (A1) that (1) $|\psi_i(1)\rangle$ occurs only once and $|\phi_i(2)\rangle$ occurs only once too ($i=1-s$) and (2) the number of terms is at most d, feature which is in much contrast with that in the trivial expression above. Equation (A1) is termed the Schmidt decomposition of the state $|\Psi\rangle$. The number s, the number of terms in the Schmidt decomposition in Eq. (A1), ranges from unity to d and is termed the Schmidt rank of the state $|\Psi\rangle$. The positive numbers p_i^Ψ $(i=1,2,\ldots,s)$ are referred to as the Schmidt coefficients of the state $|\Psi\rangle$ and satisfy the normalization relation

$$\sum_{i=1}^{s}p_i^\Psi=1. \tag{A2}$$

The entanglement measures for the state $|\Psi\rangle$ are derived from the set of Schmidt coefficients for the state $|\Psi\rangle$, $\{p_i^\Psi|i=1,2,\ldots,s\}$. For example, the entanglement entropy of the state $|\Psi\rangle$, denoted by $S_{\rm en}(|\Psi\rangle)$, is derived as,

$$S_{\rm en}(|\Psi\rangle)=-\sum_{i=1}^{s}p_i^\Psi\left(\log_2 p_i^\Psi\right). \tag{A3}$$

See Eq. (31) in Ref. [3].

The Schmidt decomposition in Eq. (A1) applies to any two-particle system whether the particles are identical or not.

We can determine from the Schmidt rank s of the state $|\Psi\rangle$ whether or not the state is entangled if the particles are not identical: (i) if $s = 1$, the state $|\Psi\rangle$ is not entangled, in which case $S_{\rm en}(|\Psi\rangle) = 0$, and (ii) if $s > 1$, the state $|\Psi\rangle$ is entangled, in which case $S_{\rm en}(|\Psi\rangle) > 0$. The entanglement entropy of the state $|\Psi\rangle$ is a measure of entanglement of the state $|\Psi\rangle$ for systems composed of two nonidentical particles. It ranges from zero to $\log_2 d$, where "zero" refers to nonentangled states, as mentioned just above, and "$\log_2 d$" refers to the maximally entangled state.

For systems composed of two identical particles, the characteristic construction due to the indistinguishability of those identical particles would occur in the Schmidt decomposition. Special attention should be hence paid to the criterion for determining whether or not the state $|\Psi\rangle$ is entangled and measures of entanglement of the state $|\Psi\rangle$. In the next section, we discuss entanglement in two-electron systems in this respect.

2. Entanglement in two-electron systems

We consider states of a two-electron system composed of electrons 1 and 2. We prepare two d-dimensional linear spaces $\mathcal{H}(1)$ and $\mathcal{H}(2)$ of one-electron states involved for electrons 1 and 2, respectively, as in Appendix, Sec. 1. As both particles are identical, $\mathcal{H}(1)$ and $\mathcal{H}(2)$ are the same if we omit the electron label. We hence take one more d-dimensional linear space $\mathcal{H}$, which is obtained with simply omitting the electron label in $\mathcal{H}(1)$ [$\mathcal{H}(2)$]. Because of the indistinguishability of electrons, the state $|\Psi\rangle$ [$\in \mathcal{H}(1) \otimes \mathcal{H}(2)$] is antisymmetric with respect to the permutation operator of electrons 1 and 2. Equation (A1) may be rewritten in the form such that Slater determinants occur as a result [24,25]:

$$\begin{aligned}|\Psi\rangle &= \sum_{i=1}^{s/2} \alpha_i^{\Psi} \frac{1}{\sqrt{2}} [|\upsilon_{2i-1}(1)\rangle|\upsilon_{2i}(2)\rangle - |\upsilon_{2i}(1)\rangle|\upsilon_{2i-1}(2)\rangle] \\ &= \sum_{i=1}^{s/2} \alpha_i^{\Psi} \left(\frac{1}{\sqrt{2}} \begin{vmatrix} |\upsilon_{2i-1}(1)\rangle & |\upsilon_{2i}(1)\rangle \\ |\upsilon_{2i-1}(2)\rangle & |\upsilon_{2i}(2)\rangle \end{vmatrix} \right), \end{aligned} \tag{A4}$$

where the coefficients α_i^{Ψ} are nonzero complex numbers and the set of one-electron states involved $\{|\upsilon_i\rangle | i = 1, 2, \ldots, d\}$ is an adequate orthonormal basis for $\mathcal{H}$. The Schmidt rank s is an even number since the summation is taken from $i = 1$ to $s/2$. The decomposition of the state $|\Psi\rangle$ in Eq. (A4) is termed the Slater decomposition of the state $|\Psi\rangle$ [24,25]. The set of Schmidt coefficients for the state $|\Psi\rangle$ is written as

$$s(|\Psi\rangle) = \overbrace{\left(|\alpha_1^{\Psi}|^2/2,\ |\alpha_1^{\Psi}|^2/2,\ |\alpha_2^{\Psi}|^2/2,\ |\alpha_2^{\Psi}|^2/2,\ \ldots,\ |\alpha_{s/2}^{\Psi}|^2/2,\ |\alpha_{s/2}^{\Psi}|^2/2 \right)}^{s \text{ elements}}, \tag{A5}$$

where $|\alpha_1^{\Psi}|^2/2 \geqslant |\alpha_2^{\Psi}|^2/2 \geqslant \cdots \geqslant |\alpha_{s/2}^{\Psi}|^2/2 > 0$ and the set $s(|\Psi\rangle)$ is expressed in the form of a row vector. It is remarkable that any of $|\alpha_i^{\Psi}|^2/2$ ($i = 1, 2, \ldots, s/2$) occurs twice, and such a twin structure is attributed to the indistinguishability of electrons. The normalization relation in Eq. (A2) is rewritten as

$$\sum_{i=1}^{s/2} |\alpha_i^{\Psi}|^2 = 1. \tag{A6}$$

Because of the normalization relation, it follows that

$$0 < |\alpha_i^{\Psi}|^2 \leqslant 1 \quad (i = 1, 2, \ldots, s/2). \tag{A7}$$

We stress that the state composed of a single Slater determinant in the Slater decomposition in Eq. (A4) is indeed a nonentangled state though such a state appears an entangled state because it is not a product state [25]. We briefly argue the reason why the following state is nonentangled:

$$\begin{aligned} &\frac{1}{\sqrt{2}} \begin{vmatrix} |\upsilon_1(1)\rangle & |\upsilon_2(1)\rangle \\ |\upsilon_1(2)\rangle & |\upsilon_2(2)\rangle \end{vmatrix} \\ &\quad = \frac{1}{\sqrt{2}} [|\upsilon_1(1)\rangle|\upsilon_2(2)\rangle - |\upsilon_2(1)\rangle|\upsilon_1(2)\rangle]. \end{aligned} \tag{A8}$$

In this state, the state of each electron is definite, i.e., one electron is in the state $|\upsilon_1\rangle$ and the other electron is in the state $|\upsilon_2\rangle$. The state expressed as Eq. (A8) is hence nonentangled. It does not matter which electron 1 or 2 is in the state $|\upsilon_1\rangle$ or $|\upsilon_2\rangle$ because it is formal to distinguish indistinguishable electrons with labeling. Refer to Ref. [25] for more detailed reasoning. The number of the Slater determinants in the Slater decomposition in Eq. (A4), the number which is termed the Slater rank of the state $|\Psi\rangle$ [24], consequently gives a criterion for determining whether or not the state $|\Psi\rangle$ in Eq. (A4) is entangled [25]: (i) if "the Slater rank of the state $|\Psi\rangle$" = 1, the state $|\Psi\rangle$ is nonentangled, and (ii) if "the Slater rank of the state $|\Psi\rangle$" >1, the state $|\Psi\rangle$ is entangled. The indistinguishability of electrons gives the large influence on the criterion for the determination of entanglement or not.

We then find out the influence of the indistinguishability of electrons on the entanglement entropy. The entanglement entropy for the state $|\Psi\rangle$, $S_{\rm en}(|\Psi\rangle)$, is calculated from the set of Schmidt coefficients in Eq. (A5) to be

$$S_{\rm en}(|\Psi\rangle) = -\left(\sum_{i=1}^{s/2} |\alpha_i^{\Psi}|^2 \log_2 |\alpha_i^{\Psi}|^2 \right) + 1. \tag{A9}$$

As Eq. (A7) holds, we obtain

$$S_{\rm en}(|\Psi\rangle) \geqslant 1. \tag{A10}$$

The equality holds if and only if the Slater rank of the state $|\Psi\rangle$ is unity [25], i.e., if and only if the state $|\Psi\rangle$ is composed of only one Slater determinant. In such a case, the value of $S_{\rm en}(|\Psi\rangle)$ is always unity whatever the one-electron states involved in the determinant are, and the "unity" hence comes from the Slater determinant itself. It consequently follows that the invariant part "1" in the right-hand side of Eq. (A9) is attributed to the indistinguishability of electrons. The entanglement entropy has an advantage that it may be decomposed into the contribution from the indistinguishability

of electrons and that from other sources. We choose the entanglement entropy from among a various range of entanglement measures because of this advantage. From the above-mentioned discussion, we have a significant conclusion that the indistinguishability of electrons does not contribute to entanglement and the quantity

$$S_{\text{en}}(|\Psi\rangle) - 1 = -\sum_{i=1}^{s/2} \left|\alpha_i^{\Psi}\right|^2 \log_2 \left|\alpha_i^{\Psi}\right|^2 \tag{A11}$$

is a better measure of entanglement for the state $|\Psi\rangle$ than $S_{\text{en}}(|\Psi\rangle)$ itself [25]. In this paper, we use "$S_{\text{en}}(|\Psi\rangle) - 1$" as the entanglement measure for the state $|\Psi\rangle$. The entanglement measure "$S_{\text{en}}(|\Psi\rangle) - 1$" is termed the "offset" entanglement entropy for the state $|\Psi\rangle$ in this paper. The offset entanglement entropy is what expresses the amount of entanglement in two-electron systems. The offset entanglement entropy ranges from zero to $\log_2(d/2)$, where "zero" refers to nonentangled states, as mentioned above, and "$\log_2(d/2)$" refers to the maximally entangled state.

[1] A. Einstein, B. Podolsky, and N. Rosen, Phys. Rev. **47**, 777 (1935).

[2] *Entangled World: The Fascination of Quantum Information and Computation*, edited by J. Audretsch (Wiley, Hoboken, NJ, 2006).

[3] M. C. Tichy, F. Mintert, and A. Buchleitner, J. Phys. B: At., Mol. Opt. Phys. **44**, 192001 (2011).

[4] H. Miyagi, A. Ichimura, and N. Kouchi, J. Phys. B: At., Mol. Opt. Phys. **40**, 617 (2007).

[5] K. Jänkälä, P. V. Demekhin, S. Heinäsmäki, I. Haar, R. Hentges, and A. Ehresmann, J. Phys. B: At., Mol. Opt. Phys. **43**, 065104 (2010).

[6] T. Odagiri, M. Murata, M. Kato, and N. Kouchi, J. Phys. B: At., Mol. Opt. Phys. **37**, 3909 (2004).

[7] K. Hosaka, K. Shiino, Y. Nakanishi, T. Odagiri, M. Kitajima, and N. Kouchi, Phys. Rev. A **93**, 063423 (2016).

[8] K. Hosaka, Y. Torizuka, P. Schmidt, A. Knie, A. Ehresmann, T. Odagiri, M. Kitajima, and N. Kouchi, Phys. Rev. A **99**, 033423 (2019).

[9] A. Dochain, B. Fabre, C. Lauzin, and X. Urbain, Phys. Rev. A **107**, 013109 (2023).

[10] J. L. Sanz-Vicario, H. Bachau, and F. Martín, Phys. Rev. A **73**, 033410 (2006).

[11] Y. Torizuka, K. Hosaka, P. Schmidt, T. Odagiri, A. Knie, A. Ehresmann, R. Kougo, M. Kitajima, and N. Kouchi, Phys. Rev. A **99**, 063426 (2019).

[12] I. Sánchez and F. Martín, J. Chem. Phys. **110**, 6702 (1999).

[13] J. Tennyson, At. Data Nucl. Data Tables **64**, 253 (1996).

[14] T. Tanabe, T. Odagiri, M. Nakano, I. H. Suzuki, and N. Kouchi, Phys. Rev. Lett. **103**, 173002 (2009).

[15] T. Tanabe, T. Odagiri, M. Nakano, Y. Kumagai, I. H. Suzuki, M. Kitajima, and N. Kouchi, Phys. Rev. A **82**, 040101(R) (2010).

[16] Y. Nakanishi, K. Hosaka, R. Kougo, T. Odagiri, M. Nakano, Y. Kumagai, K. Shiino, M. Kitajima, and N. Kouchi, Phys. Rev. A **90**, 043405 (2014).

[17] K. Hosaka, Y. Torizuka, P. Schmidt, A. Ehresmann, T. Odagiri, M. Kitajima, and N. Kouchi, Phys. Rev. A **103**, 062809 (2021).

[18] K. Ito, Y. Morioka, M. Ukai, N. Kouchi, Y. Hatano, and T. Hayaishi, Rev. Sci. Instrum. **66**, 2119 (1995).

[19] Y. V. Vanne, A. Saenz, A. Dalgarno, R. C. Forrey, P. Froelich, and S. Jonsell, Phys. Rev. A **73**, 062706 (2006).

[20] H. Lefebvre-Brion and R. W. Field, *The Spectra and Dynamics of Diatomic Molecules* (Elsevier, Amsterdam, 2004).

[21] B. H. Bransden and C. J. Joachain, *Physics of Atoms and Molecules*, 2nd ed. (Prentice Hall, Englewood Cliffs, NJ, 2003).

[22] J. P. R. Cuartas and J. L. Sanz-Vicario, Phys. Rev. A **91**, 052301 (2015).

[23] J. D. Bozek, J. E. Furst, T. J. Gay, H. Gould, A. L. D. Kilcoyne, J. R. Machacek, F. Martín, K. W. McLaughlin, and J. L. Sanz-Vicario, J. Phys. B: At., Mol. Opt. Phys. **39**, 4871 (2006); **41**, 039801 (2008); **42**, 029801 (2009).

[24] J. Schliemann, J. I. Cirac, M. Kus, M. Lewenstein, and D. Loss, Phys. Rev. A **64**, 022303 (2001).

[25] G. C. Ghirardi and L. Marinatto, Phys. Rev. A **70**, 012109 (2004).